Solar Physics
DOI: 10.1007/•••••-•••-•••-••••-•

arXiv:0806.4424v2 [astro-ph] 30 Jun 2008

An Extreme Solar Event of 20 January 2005: Properties of the Flare and the Origin of Energetic Particles

V.V. Grechnev[1] · **V.G. Kurt**[2] · **I.M. Chertok**[3] · **A.M. Uralov**[1] · **H. Nakajima**[4] · **A.T. Altyntsev**[1] · **A.V. Belov**[3] · **B.Yu. Yushkov**[2] · **S.N. Kuznetsov**[2*] · **L.K. Kashapova**[1] · **N.S. Meshalkina**[1] · **N.P. Prestage**[5]

Received ; accepted

© Springer ••••

Abstract The famous extreme solar and particle event of 20 January 2005 is analyzed from two perspectives. Firstly, using multi-spectral data, we study temporal, spectral, and spatial features of the main phase of the flare, when the strongest emissions from microwaves up to 200 MeV gamma-rays were observed. Secondly, we relate our results to a long-standing controversy on the origin of solar energetic particles (SEP) arriving at Earth, *i.e.*, acceleration in flares, or shocks ahead of coronal mass ejections (CMEs). Our analysis shows that all electromagnetic emissions from microwaves up to 2.22 MeV line gamma-rays during the main flare phase originated within a compact structure located just above sunspot umbrae. In particular, a huge ($\approx 10^5$ sfu) radio burst with a high frequency maximum at 30 GHz was observed, indicating the presence of a large number of energetic electrons in very strong magnetic fields. Thus, protons and electrons responsible for various flare emissions during its main phase were accelerated within the magnetic field of the active region. The leading, impulsive parts of the ground-level enhancement (GLE), and highest-energy gamma-rays identified with π^0-decay emission, are similar and closely correspond in time. The origin of the π^0-decay gamma-rays is argued to be the same as that of lower-energy emissions, although this is not proven. On the other hand, we estimate

[1] Institute of Solar-Terrestrial Physics SB RAS, Lermontov St. 126A, Irkutsk 664033, Russia
(e-mail: grechnev@iszf.irk.ru)
[2] Skobeltsyn Institute of Nuclear Physics Moscow Lomonosov State University, Moscow, 119992 Russia
[3] Pushkov Institute of Terrestrial Magnetism, Ionosphere and Radiowave Propagation (IZMIRAN), Troitsk, Moscow Region, 142190 Russia
[4] Nobeyama Radio Observatory, Minamimaki, Minamisaku, Nagano 384-1305, Japan
[5] IPS Radio and Space Services Culgoora Solar Observatory, Australia

the sky-plane speed of the CME to be 2 000 – 2 600 km s^{-1}, *i.e.*, high, but of the same order as preceding non-GLE-related CMEs from the same active region. Hence, the flare itself rather than the CME appears to determine the extreme nature of this event. We therefore conclude that the acceleration, at least, to sub-relativistic energies, of electrons and protons, responsible for both the major flare emissions and the leading spike of SEP/GLE by 07 UT, are likely to have occurred nearly simultaneously within the flare region. However, our analysis does not rule out a probable contribution from particles accelerated in the CME-driven shock for the leading GLE spike, which seemed to dominate at later stages of the SEP event.

Keywords: Coronal Mass Ejections; Cosmic Rays; Energetic Particles; Flares; Particle Acceleration; Radio Bursts; X-Ray Bursts

1. Introduction

The solar eruptive-flare event of 20 January 2005 has attracted great attention from the solar and solar-terrestrial community due to its outstanding characteristics (see, *e.g.*, http://creme96.nrl.navy.mil/20Jan05/). Despite its occurrence at the deep descending phase of the solar cycle, the event was characterized, in particular, by strong gamma-ray emission with a photon energy up to at least 200 MeV; by one of the strongest microwave bursts with a spectral maximum frequency $\approx$ 30 GHz, by a fast halo coronal mass ejection (CME), and was accompanied by a very hard-spectrum solar energetic particle (SEP) flux near Earth including the second largest ground-level enhancement (GLE) of cosmic ray intensity in observational history.

Many studies are devoted to this extreme event, but they mainly concern the cosmic ray aspect. The central points of these studies are the features and origin of the SEP/GLE. Additionally, a long-standing discussion over the origin of accelerated protons in solar events, *i.e.*, CME-driven shock-acceleration or flare-acceleration, has been strengthened. In particular, Gopalswamy *et al.* (2005) estimated that the CME had the largest sky-plane speed exceeding 3000 km s^{-1} and concluded that the GLE had a shock origin. On the other hand, Simnett (2006, 2007) considered the relative timing of various manifestations in this event and several other factors, and stated that the CME was not responsible for the relativistic ion acceleration. Kuznetsov *et al.* (2005a,b, 2006a,b, 2007) also argued in favor of flare-related proton acceleration in this and other events.

These contradicting opinions reflect a long-standing controversy over different viewpoints of the origin of high-energy protons related to solar events [see Cliver (2000) for a historical review]. Many papers have been published in support of each of these opposing viewpoints. Some researchers insist that all energetic particles arriving at Earth are accelerated exclusively by CME-driven shocks, rather far from flare regions (Reames, 1999; Kahler, 2001). Some others argue

*Deceased 17 May 2007

that traveling shocks could perhaps contribute to lower-energy proton fluxes ($E < 10$ MeV), while higher-energy ones ($E > 100$ MeV) are flare-accelerated on the Sun (*e.g.*, Klein and Trottet, 2001; Chertok, 1995; Livshits and Belov, 2004; Li *et al.*, 2007a,b).

The 20 January 2005 event provides a unique chance to address this problem for the following reasons: (a) availability of spectral-imaging gamma-ray data from the Reuven Ramaty High Energy Solar Spectroscopic Imager (RHESSI; Lin *et al.*, 2002), (b) availability of highest-energy spectral gamma-ray data up to 200 MeV from the non-imaging SOlar Neutron and Gamma experiment (SONG; Kuznetsov *et al.*, 2004, 2008) on board the CORONAS-F spacecraft (Oraevsky and Sobelman, 2002), (c) the strongest GLE in over half a century of observations, caused by the unusually prompt arrival of protons at Earth (Bieber *et al.*, 2005; Belov *et al.*, 2005; Simnett, 2006; Cliver, 2006), and (d) availability of many other kinds of observational data, for both the flare region on the Sun, and for the near-Earth space, up to the Earth's surface. In particular, the source region on the Sun was observed in soft X-rays (SXR) by GOES-10 and GOES-12 including the Soft X-ray Imager (SXI; Hill *et al.*, 2005). The Hα flare was recorded at the IPS Culgoora Solar Observatory in Australia and at the Hiraiso Observatory in Japan. Nobeyama Radio Polarimeters (NoRP; Nakajima *et al.*, 1985; Torii *et al.*, 1979) recorded an unusually strong microwave burst at six frequencies: 2, 3.75, 9.4, 17, 35, and 80 GHz. The Transition Region and Coronal Explorer (TRACE; Handy *et al.*, 1999) observed the flare after its peak in the 1600 Å channel. The Extreme-Ultraviolet Imaging Telescope (EIT; Delaboudinière *et al.*, 1995) and the Large-Angle Spectrometric Coronagraph (LASCO; Brueckner *et al.*, 1995) on SOHO also supplied images related to this event.

In this paper, we first analyze in detail the flare itself. We consider its source region on the Sun in different spectral domains, using available imaging data and reconciling time profiles of various emissions as well as spatial and spectral characteristics of their sources. In this way, we endeavor to understand this remarkable flare, its configuration, and the physical conditions in the flare region. Then, based on the results of this analysis, we consider which of the two above-mentioned models of the origin of high-energy protons better matches observations of the 20 January 2005 event. Our methodology is based on joint analysis of multi-spectral data. To minimize the influence of instrumental effects and model-dependent estimations, we verify our results and estimates by using different methods and independent observations as much as possible. Their agreement enhances the reliability of our results and conclusions. Is is important to analyze manifestations of accelerated protons primarily during their main peak (corresponding to the main phase of the highest rate of flare energy release), when the influence of subsequent post-eruptive processes and transport effects on the Sun and/or in interplanetary space, as well as probable contributions from different acceleration mechanisms, which are difficult to distinguish, is minimal.

We start our consideration in Section 2 with observational solar data and their brief analysis, including the development of the active region and pre-flare situation. Then, flare manifestations in gamma-rays, hard and soft X-rays, microwaves, Hα, 1600 Å, and extreme-ultraviolet (EUV) emissions, as well as

the CME are addressed. We conclude that the extreme features of the flare were due to its occurrence in the strong magnetic fields just above sunspot umbrae. Section 3 is devoted to relating flare features to the observed SEP/GLE characteristics. In particular, its proton productivity is compared with other events from the same active region. Finally, the temporal parameters of the impulsive parts of the gamma-ray burst and GLE are compared. The same population of energetic particles appears to be responsible for both the π^0-decay gamma-ray burst and the leading spike of the GLE. In turn, the π^0-decay emission was close, but not identical to, emissions whose sources were located within the solar active region. In Section 4, we discuss the results of our analysis and argue that the π^0-decay emission also originated in the flare region and that data available to us appear to favor the flare-related initial acceleration of particles responsible for the leading GLE spike, but do not preclude their origin in a CME-driven shock. Section 5 summarizes the results of our analyses of the flare and origin of SEP/GLE particles and briefly addresses their implications.

2. Observations and Analysis

The eruptive solar event of 20 January 2005 had several outstanding properties. Many solar events are known, but only a small number of them are comparable with this event in some of its features. The high-energy near-Earth proton enhancement was unprecedented. Since 1975, more than 600 proton events with $E_{\mathrm{P}} > 100\,\mathrm{MeV}$ have been registered; however, high-energy proton fluxes exceeded 100 pfu in only five events. On 20 January 2005, the peak flux for $E_{\mathrm{P}} > 100\,\mathrm{MeV}$ protons reached the record value of 650 pfu. At lower energies, the near-Earth proton flux was not extremely intense, about 2000 pfu. A very strong, collimated high-energy beam-like proton stream arrived at the Earth's orbit almost simultaneously with electromagnetic flare emissions and produced the GLE, which was the largest one in the last solar cycle and one of the largest ever observed (Belov *et al.*, 2005; Simnett, 2006; Bieber *et al.*, 2005; Cliver, 2006). The largest effect, by an order of magnitude, was recorded with antarctic neutron monitors.

Strong hard X-ray (HXR) and pronounced gamma-ray emissions up to 17 MeV were recorded with RHESSI (Krucker, Hurford, and Lin, 2005; Hurford *et al.*, 2006b; Share *et al.*, 2006). CORONAS-F/SONG detected gamma-rays of >100 MeV. Only a few solar events are known in which such high-energy gamma-rays have been recorded (*e.g.*, Ryan, 2000).

The CME launched in this event was well observed with SOHO/LASCO in only one C2 frame at $\approx 4.4 R_{\odot}$ (06:54[1]). Subsequent LASCO frames are severely contaminated with traces of energetic particles; thus, the CME speed is rather uncertain. Gopalswamy *et al.* (2005) estimated it to be up to 3242 $\mathrm{km\,s^{-1}}$, and the estimate of Simnett (2006) was 2500 $\mathrm{km\,s^{-1}}$.

The microwave burst was huge, up to $\approx 10^5$ sfu, and was observed up to 80 GHz. The associated long-duration flare was strong, but not extraordinary, both

[1]Times hereafter are UT, if otherwise not specified

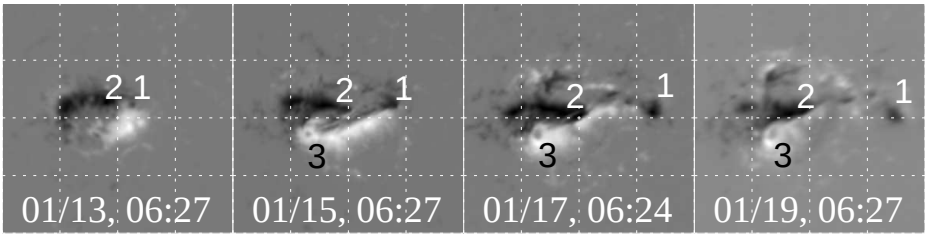

Figure 1. Evolution of AR 10720: SOHO/MDI magnetograms for 13 – 19 January. Field of view is $295'' \times 295''$. Labels 1 – 3 mark features discussed in the text.

in soft X-ray and Hα emissions (X7.1/2B). We analyze the properties of this superevent and show some of them to be interrelated.

2.1. History of the Active Region and Pre-Flare Situation

The event of 20 January 2005 occurred in active region 10720 (N14 W60). This region evolved rapidly. Its evolution is shown by photospheric magnetograms observed with the Michelson Doppler Imager (MDI; Scherrer *et al.*, 1995) on SOHO. Figure 1 presents a set of MDI magnetograms of AR 10720 from 13 through 19 January. Differential rotation is compensated to 15 January, 00 UT. The magnetograms show two major domains, the northern one of S-polarity (dark), and the southern one of N-polarity (bright).

From 15 January onwards, the maximum magnetic field strength exceeded the measurable capabilities of the MDI[2]. This shows up as a darker patch *3* within the bright N-polarity domain. On 20 January, the active region was not far from the limb, leading to significant distortions of the magnetograms. We therefore refer to a magnetogram obtained on 18 January[3]. On this day, the maximum strength in a "non-saturated" part of the N-polarity area reached +3120 G, while the persistence of patch *3* in this area suggests the magnetic field to be even stronger there. The maximum strength in the S-polarity area was −2700 G.

Noticeable during 13 – 20 January are (1) large shear motion along the neutral line, clearly visible from the westward drift of the westernmost S-polarity spot *1*, and (2) the displacement of the large northern S-polarity domain *2* southwards, approaching the N-domain, while the latter maintained its latitude. This convergence brought the opposite-polarity areas into contact on 17 January. These features of its development suggest the high flare productivity of AR 10720 (cf., *e.g.*, Birn *et al.*, 2000). Indeed, it produced 17 M-class and 5 X-class events from 14 through 23 January. Many of these were associated with CMEs.

Figure 2 presents the pre-flare situation in white light (WL) and at 1600 Å (TRACE), along with a magnetogram. Coordinates are referred to RHESSI pointing. The TRACE absolute pointing coordinates have an uncertainty larger than its spatial resolution[4], whereas those of RHESSI are believed to be accurate

[2]often referred to as "high field saturation", see http://soi.stanford.edu/data/cal/

[3]We use MDI magnetograms recalibrated in 2007

[4]see http://trace.lmsal.com/Project/Instrument/cal/pointing.html
and http://trace.lmsal.com/tag/

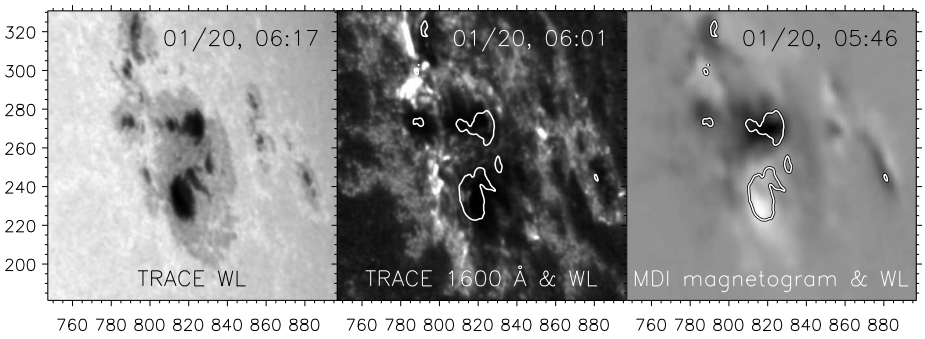

Figure 2. Pre-flare situation. TRACE WL image (left); TRACE 1600 Å image (middle) and SOHO/MDI magnetogram (right) overlaid with contours of the sunspot umbrae visible in the WL image. All images are "co-rotated" to 06:52:30 UT. Axes in all images hereafter show the distance in arcsec from the solar disk center.

(and we checked this by comparing TRACE WL and a full-disk MDI continuum image). The information required to accurately coalign TRACE and RHESSI images was obtained in the course of our analysis (Section 2.2.3).

The area of the largest N-polarity sunspot's umbra is about 1.74 larger than the largest S-polarity one. All of these properties of the sunspots imply that the real magnetic field is probably stronger in the N-polarity umbra, while its total magnetic flux is certainly larger.

The evolution of AR 10720 clearly points to a high flare productivity, which indeed took place. Its magnetic fields reached extreme strengths. The active region became "ready" to produce its strongest flare.

2.2. Manifestations in the Lower Solar Atmosphere and Hard Electromagnetic Emissions

2.2.1. Hard X-ray and Gamma-Ray Time Profiles

The event was observed in X-rays and gamma-rays by RHESSI[5] and CORONAS-F/SONG. Panels a – c of Figure 3 show some of the wide-band RHESSI time profiles (four second sampling rate) produced using RHESSI Data Analysis Software. The time profiles in a range of 3 – 25 keV (*e.g.*, panel *a*) are similar and smooth, with their maxima significantly delayed with respect to those of higher energies, most likely due to the Neupert effect, which we discuss later. Harder emissions became strong at 06:42:40, while softer X-ray emissions started earlier, probably due to initial heating. The time profiles in a range of 25 – 300 keV are similar. They seem saturated around the flare peak (this effect can be compensated for, see Section 2.2.2). The highest-energy time profiles (not shown) lag behind those of 25 – 300 keV and rise sharply after 06:45.

SONG observed hard emissions in 12 channels from 43 keV to 310 MeV with a one second sampling rate (Figure 3c – f). Its net count rates were computed

[5]RHESSI data used in this paper are preliminary.

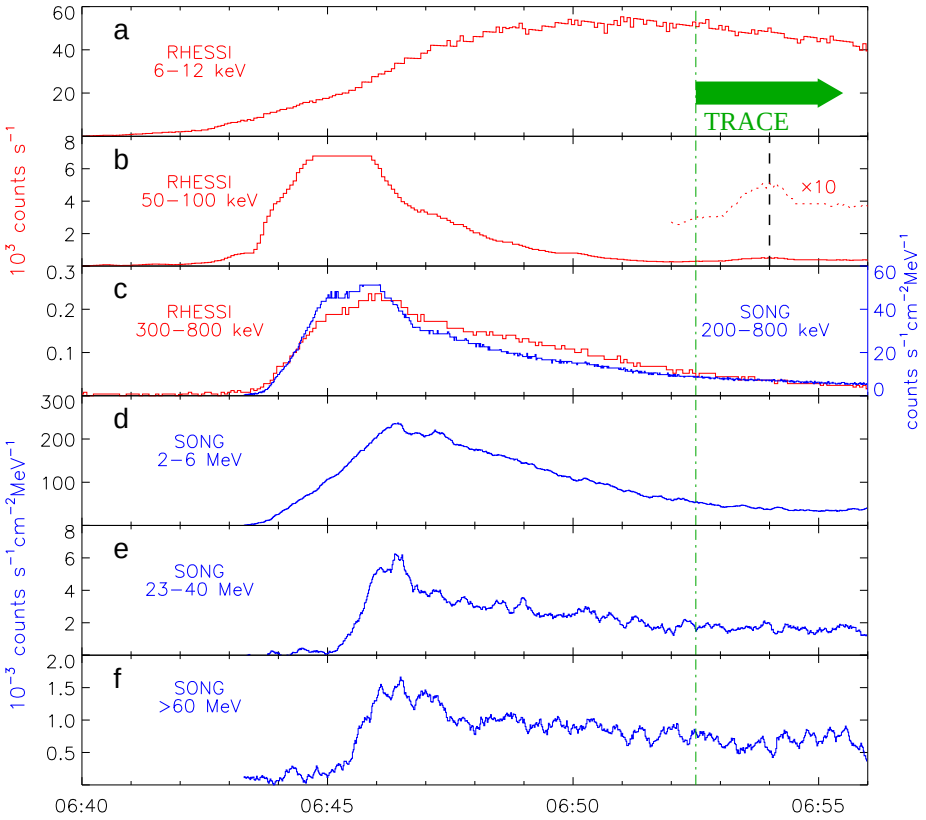

Figure 3. a – c: Some wide-band RHESSI time profiles (red). Green dash-dotted line shows start of TRACE observations. Black dashed line marks a weak enhancement of 25 – 300 keV emission. Red dotted line shows part of its time profile enlarged ten-times. c – f: Some SONG time profiles smoothed over 13 points (blue; the 200 – 800 keV channel has not been smoothed).

by subtracting background trends inferred from previous orbits. The gamma-ray burst was reliably recorded from 06:43:30 to 06:58:30, then uncertainties become large due to contamination from charged particles reaching the spacecraft. The 43 – 230 keV channels suffer from register overflow. Flux variations recorded with RHESSI and SONG in corresponding energy bands are close, any dissimilarities are probably due to differences in energy bands. The differences in count rates (*e.g.*, panel *c*) are due to different detectors. Two peaks at about 06:45 and 06:46 are detectable in the records of both instruments. The hardest emissions rise sharply after 06:45:30.

The time profiles in 50 – 100 keV and 200 – 800 keV bands are largely similar. These time profiles and the highest-energy (> 60 MeV) emissions have some similarities as well as differences. The highest-energy gamma-rays start later than lower-energy emissions, rise sharper, and decay slower. On the other hand, subsidiary peaks in the > 60 MeV band at 06:46, 06:46:30, and 06:47:15 have pronounced counterparts in lower-energy bands. They are also detectable in intermediate-energy bands, which are not shown.

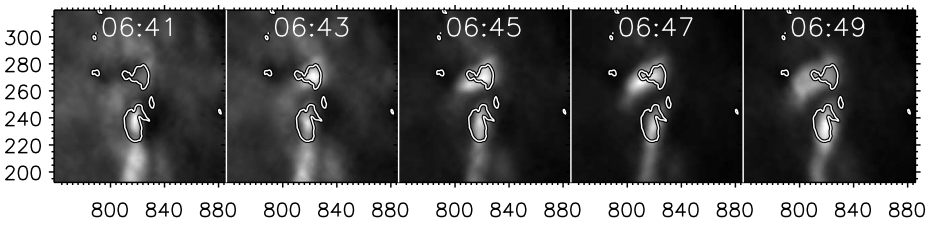

Figure 4. Development of flare ribbons in Hα emission. Contours show the sunspot umbrae.

2.2.2. Hα, White Light, and Hard X-ray Images

Culgoora Solar Observatory observed the Hα flare every 20 seconds from 06:40:47 to 08:04. Figure 4 shows some of these images overlaid with contours of the sunspot umbrae from the TRACE WL image (see Figure 2). One can see the development of Hα flare ribbons with respect to sunspots starting from the onset of the HXR emission up to its cessation (maximum of SXR emission). Initially, Hα emission comes from the future southern ribbon, being concentrated in the sunspot umbra. The emission south of this sunspot is due to weaker initial flaring. At 06:43, when HXR emission becomes strong, Hα emission appears in the northern sunspot umbra. Later on, the northern ribbon was significantly extended toward the southeast.

The limited resolution of the Hα images and atmospheric effects do not permit consideration of bright kernels, but it is possible to study larger features. Figure 5a shows time profiles of the total Hα emission computed separately for each ribbon. Their similarity suggests a single common source for their emissions.

Figure 6 shows the relative positions of 50 – 100 keV HXR sources, sunspots, and flare ribbons around the time of the main flare phase. At 06:40:45, both HXR sources are located in the sunspot umbrae. The active northern source shifts firstly east along the ribbon, and then, when HXR flux sharply increases, it returns to the umbra. Then, it extends along the ribbon, and during the maximum phase moves to the east. The southern source is much steadier.

HXR sources are located on the Hα ribbons. Similar development of the flare ribbons and HXR sources is also shown by a movie of this event[6], TRACE 1600 Å + RHESSI/SXR & HXR. Hα and HXR images show the following features: (a) both ribbons cross the umbrae of sunspots, (b) initially, HXR and Hα emission sources are located in the sunspot umbrae, and then, after 06:45, the northern source shifts from the umbra to a region of weaker magnetic fields; *the gamma-ray emission maximum occurs just at this time*, and (c) the displacements of the southern HXR and Hα sources are relatively small.

To compute spatially-resolved HXR time profiles, we produced 50 – 100 keV RHESSI images using the Pixon method. Figure 5b shows HXR time profiles computed separately for each ribbon. Again, the time profiles of both ribbons are so similar as to suggest a common source for their emissions. The Hα time profiles are much smoother than those of HXR and lag behind them due to the well-known long decay time of Hα emission.

[6]http://svs.gsfc.nasa.gov/vis/a000000/a003100/a003162/

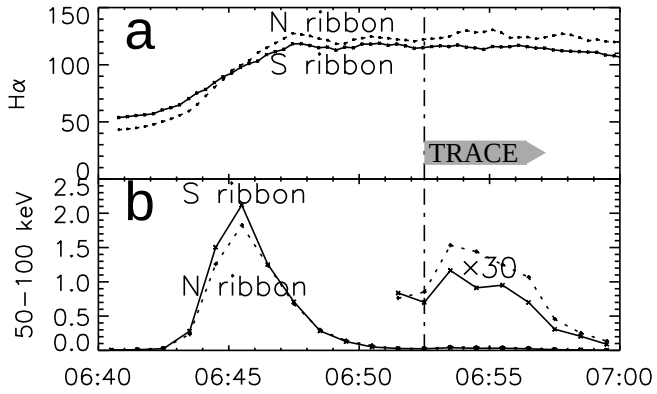

Figure 5. Time profiles of the average brightness (arbitrary units) computed separately for northern (dotted) and southern (solid) ribbons: Hα (a, Culgoora Solar Observatory), 50 – 100 keV hard X-rays (b, RHESSI). Dash-dotted line: start of TRACE observations. Enlarged time profiles show a weak enhancement of the HXR emission around 06:55.

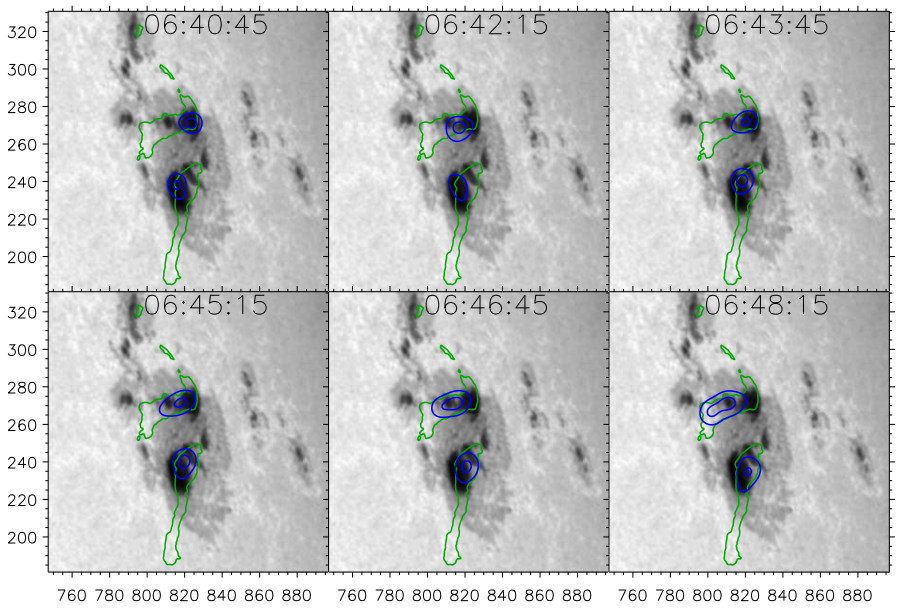

Figure 6. 50 – 100 keV hard X-ray sources (RHESSI, integration time 30 seconds, blue contours) overlying the TRACE WL image (gray scale). Green contours delineate flare ribbons in TRACE 1600 Å image at 06:52:30. All images are referred to RHESSI pointing.

2.2.3. 1600 Å and Hard X-Ray Images

The TRACE 1600 Å channel is sensitive to emissions from 4 000 – 10 000 K plasmas; hence the brightest features in Hα and 1600 Å images show basically the same structures, *i.e.*, footpoint regions of flaring coronal loops and, sometimes, the cooled loops themselves. Precipitation of high-energy electrons in the chromosphere causes its local heating, HXR bremsstrahlung, and the excitation

of Hα and 1600 Å emissions from lower layers of the solar atmosphere. Therefore, a correlation is expected between the positions and time profiles of HXR and 1600 Å sources. TRACE had a break in observations between 06:18 and 06:52:30; afterwards, it showed well-developed flare ribbons.

Using variance and correlation analyses (Grechnev, 2003; Slemzin, Kuzin, and Bogachev, 2005) of TRACE 1600 Å images observed during 06:52:41 – 06:57:30, we revealed several pairs of kernels with variable brightness (cf. Su *et al.*, 2006). The paired kernels, located in different ribbons with similar time profiles, suggest a common source of precipitated electrons. They most likely represent conjugate footpoints of the loops connecting them (cf. Grechnev, Kundu, and Nindos, 2006). Unlike the main phase of the flare, the kernels were located at the outer sides of the ribbons, far from the sunspot's umbrae. This outward motion corresponds to the expansion of the ribbons.

We then performed the variance and correlation analyses for the RHESSI 50 – 100 keV images produced using the CLEAN method over the same time interval, when the HXR emission was enhanced (see Figures 3, 5). It revealed regions with a configuration corresponding closely with the TRACE 1600 Å kernels, but displaced by $[+7.5'', -10.5'']$. This provided us with the information required to coalign TRACE and RHESSI images with an accuracy of the order of $\approx 1''$. This also confirms that the ribbons represent the bases of closed loops.

As established in Sections 2.2.1 – 2.2.3, *atypically, the flare ribbons in this event crossed the sunspot umbrae. The coronal configuration above the ribbons was closed. During the main phase, the brightest Hα and HXR emissions came from the sunspot umbrae. The flare occurred in very strong magnetic fields.*

2.2.4. HXR and Gamma-Ray Spectra and Images

As Figure 3 shows, the spectrum became harder after 06:45 UT. Figure 7 presents the non-thermal parts of the spectra recorded with RHESSI and SONG just after the flare peak. The detailed RHESSI spectrum was computed using the OSPEX software. The SONG spectrum (Kuznetsov *et al.*, 2007) extends up to the highest energies. Data from both instruments largely agree with each other quantitatively; however, the lowest SONG band suffers from overflow, while the absolute calibration of highest-energy RHESSI data is preliminary. One can distinguish several components in both spectra. These components correspond to the expected electron-bremsstrahlung and nuclear gamma-ray features.

The power-law index of bremsstrahlung is $\gamma = 2.8 - 2.9$, which corresponds to an electron index of $\delta = 4.4 - 4.5$ under thick-target conditions.

The RHESSI spectrum shows a prompt electron-positron annihilation line of 511 keV and a delayed neutron-capture line of 2.22 MeV. The most intense is the discrete 2.22 MeV line, which is emitted in neutron capture on hydrogen. Neutrons appear in nuclear reactions of accelerated ions, streaming down to the photosphere, with its material. Neutrons undergo thermalization in ≈80 seconds, and some of them are eventually captured on hydrogen, $\mathrm{H} + n \rightarrow 2\mathrm{H} + \gamma$, with the emission of a 2.22 MeV photon. Thus, the discrete 2.22 MeV line is indicative of accelerated ions with an energy exceeding a few MeV.

The SONG spectrum reveals an enhancement at the highest energies, $E_\gamma >$ 60 MeV, due to Doppler-broadened emission of π^0 decay into two photons

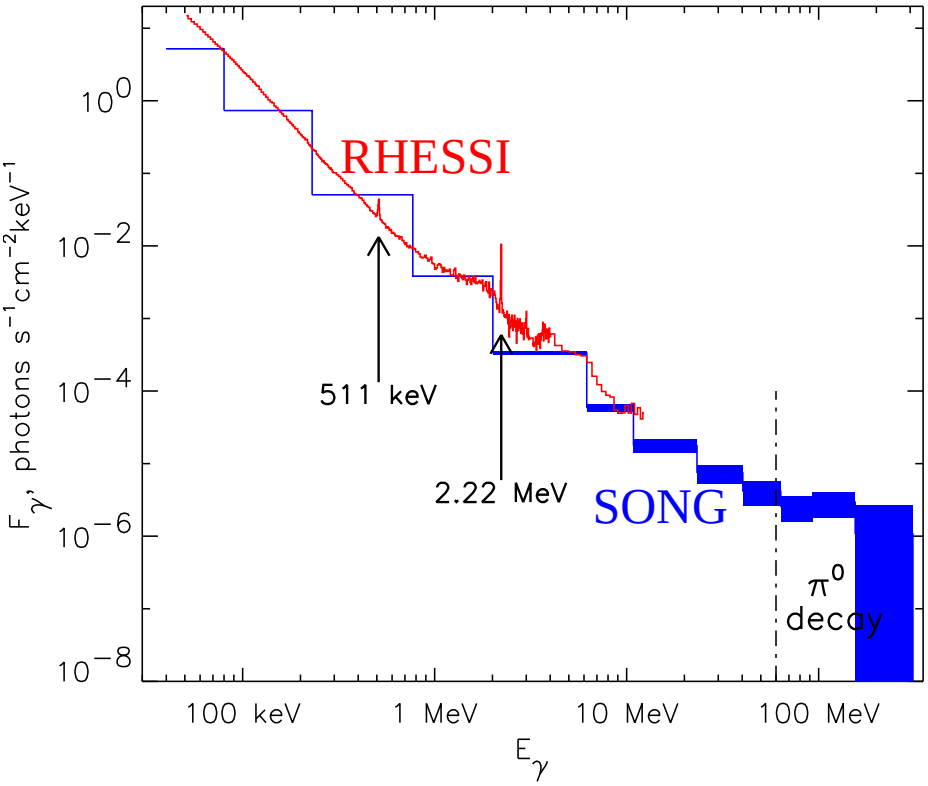

Figure 7. High-resolution RHESSI (red) and wide-range SONG (blue) spectra recorded during the hardest flare emission. Vertical dash-dotted line shows the high-energy part of the SONG spectrum where the π^0-decay emission dominates. Shading shows uncertainties.

(Kuznetsov *et al.*, 2007). The neutral pions appear in proton-proton collisions when $E_{\rm P} > 300$ MeV (Ramaty, Kozlovsky, and Lingelfelter, 1975; Hudson and Ryan, 1995). The π^0-decay emission leads the 2.22 MeV line emission by about 80 seconds (see Figure 14), which is consistent with the idea that the populations of incident protons responsible for these emissions were close.

The discrete 2.22 MeV line emission, which is indicative of the precipitation of accelerated protons and heavier ions, is strong enough to allow one to construct an image of its source. We computed it from RHESSI data using the Pixon method. To compare it with the bremsstrahlung component, we also produced a RHESSI image in a band of 100 – 300 keV for the interval of 06:46:00 – 06:46:30 using the Pixon method. This imaging interval corresponds to strong high-energy gamma-ray emission. Positions and configurations of HXR sources at 50 – 100 keV and 100 – 300 keV are close for as long as they are detectable (see Hurford *et al.*, 2006b; Share *et al.*, 2006).

Figure 8a presents the RHESSI 100 – 300 keV image (blue contours), along with green contours indicating flare ribbons (from TRACE 1600 Å image at 06:52:30 UT), on top of the TRACE WL image shown as halftone background. A large 2.22 MeV line source (beam size $\approx 35''$) is located within the active region

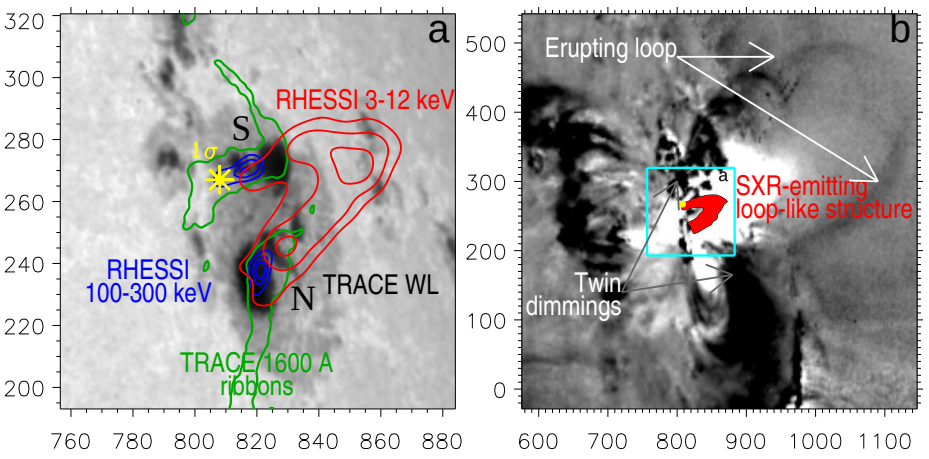

Figure 8. (a) Contours of RHESSI HXR, SXR, and gamma-ray images overlying the TRACE WL image at 06:00 shown as gray scale background. Yellow star: 2.22 MeV line centroid (1σ error size), blue contours: 100 – 300 keV image at 06:46:00 – 06:46:30, [20, 50, 80]%; red contours: 3 – 25 keV, 06:41:00 – 06:48:30, [30, 50, 80]%; green contours: flare ribbons from TRACE 1600 Å image at 06:52:30. "N" and "S" denote polarities of the main magnetic domains. (b) Dimmings revealed from EIT 195 Å images and the loop-like structure (red) visible in the EIT 171 Å band. Turquoise frame: field of view of panel (a).

with its centroid (yellow star) being in the northern ribbon. The positions of the sources in Figure 8a agree with those presented by Hurford *et al.* (2006b).

When gamma-ray emission reached its maximum, the northern HXR source became extended, with its eastern part coincident with the 2.22 MeV source. Independent of instrumental limitations and collimation of particle streams, the fact that the 2.22 MeV line source centroid was aligned with a flare ribbon means that *accelerated ions precipitated in the region, where coronal structures were closed at that time.*

2.3. Coronal Manifestations and Soft X-Ray Emission

2.3.1. Soft X-Ray RHESSI, GOES/SXI, and SOHO/EIT Images

A large loop-like SXR-emitting structure with its top reaching a height of ≈ 40 000 km and legs rooted in both sunspot umbrae is observed with EIT in the 171 Å channel, RHESSI in the 3 – 25 keV bands (Figure 8a,b), and GOES/SXI. The fact that these instruments each show a similar structure confirms its coronal nature and predominantly thermal emission. The coronal structure looks like a single thick loop with a blob-like enhancement at its top, or above it, visible in RHESSI images produced using the CLEAN method. To study this blob in detail is beyond the scope of this paper. The loop-like structure is hot, as RHESSI and GOES/SXI show, and probably consists of a bundle of thinner SXR-emitting loops. At least half an hour before the flare maximum, RHESSI detected the blob at its top (a gradual increase of SXR flux started at 06:00 according to GOES-10 and GOES-12), and then its legs became detectable. Around the flare

peak in soft X-rays, the emission from the whole Sun was dominated by this large loop-like structure. It was detectable in SXI images up to at least 08 UT and then its emission gradually declined.

To estimate its parameters, we produced a spectrum from RHESSI averaged data over 06:46 – 06:47 using OSPEX software. Then, we fitted the spectrum with a single thermal component dominating up to 25 – 30 keV, and a single power-law component. These estimations provide a temperature of $T_e \approx 32$ MK and a total emission measure of EM$\approx 7.6 \times 10^{49}$ cm^{-3}.

After 07 UT, an apparently expanding arcade appears in 1600 Å, Hα, and EUV images well below the large SXR-emitting structure. The loops of this arcade are detectable in SOHO/EIT and GOES/SXI images up to the end of the day. This arcade does not seem to be directly associated with the SXR-emitting loop-like structure. The paired kernels revealed from the analysis of HXR and 1600 Å images during the enhancement around 06:55, well after the main flare peak, do not coincide with the footpoints of the loop-like structure and most likely show the formation of the arcade underneath.

From 06:54 onwards, SOHO/EIT and LASCO frames become increasingly contaminated by the traces of high-energy particles impacting the CCD detector (cf. Andrews, 2001), and after 07:14 the images become indecipherable. This effect indicates that protons with $E_P > 40$ MeV and up to at least 400 MeV reached SOHO (Didkovsky *et al.*, 2006). Nevertheless, it is possible to reveal the structure of the coronal dimming using several frames (Grechnev, 2004; Chertok and Grechnev, 2005). Figure 8b shows a dimming "portrait" composed of minima over each pixel in the EIT 195 Å fixed-base (06:24:10) difference frames from 06:36 through 09:19 UT (this EIT channel has a temperature sensitivity maximum at 1.3 MK). Dimmings are seen as rather large, dark areas, while the red-filled contour shows a bright, overexposed image of the loop-like structure recorded in the EIT 171 Å channel. "Twin" dimmings are located near the ends of the post-eruptive arcade (here its image is inside a bright area) northwest and southwest of the ribbons and the large loop-like structure (cf. Figure 8a). The 2.22 MeV line source, like the other major flare sources, is located far from the dimming regions.

2.3.2. Soft X-Ray GOES Light Curves and the Neupert Effect

Figure 9 shows in panel (a) soft X-ray light curves recorded with GOES-10 (dashed) and GOES-12 (solid). We have computed a total emission measure EM (b) and an average temperature T_e (c) from two GOES bands (White, Thomas, and Schwartz, 2005). These values over 06:46 – 06:47 are close to those computed from RHESSI data for the same time interval. Because the large loop-like structure alone produced practically the whole solar SXR emission around the flare peak, we estimate the plasma density in this structure (Figure 9d) taking its parameters from SXR images, *i.e.*, width of a leg $\approx 9 \times 10^8$ cm, footpoint separation $\approx 2.5 \times 10^9$ cm, height $\approx 4 \times 10^9$ cm, volume $\approx 3.5 \times 10^{27}$ cm^3, and a visible area of the whole loop, 4×10^{18} cm^2.

Figure 9e shows a comparison of the unsaturated 300 – 800 keV RHESSI time profile with a temporal derivative of the SXR flux recorded in the GOES-10 1 – 8 Å channel. Their similarity shows the Neupert effect (Neupert 1968),

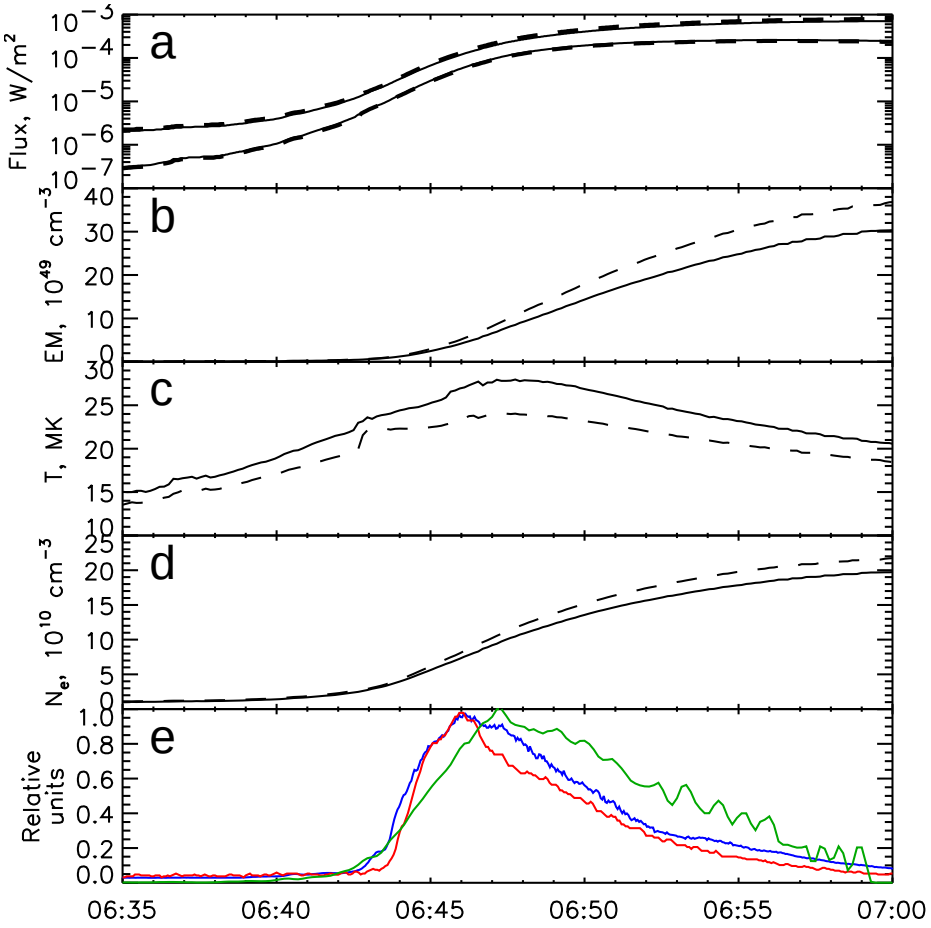

Figure 9. GOES-10 (dashed) and GOES-12 (solid) soft X-ray flux density (a), emission measure (b), temperature (c), and density (d). (e) Neupert effect. Normalized time profile of the 300 – 800 keV (red) emission in comparison with microwaves at 35 GHz (blue) and a derivative of the soft X-ray flux at 1 – 8 Å (GOES-10, green).

suggesting that the SXR-emitting plasmas "evaporated" from the chromosphere due to energy lost by precipitating high-energy particles, which produced the observed HXR emission (see also Liu *et al.*, 2006). Since the whole SXR flux came from the loop-like structure with its footpoint regions coinciding with HXR sources, and the Neupert effect proves the connection between HXR and SXR emissions, we conclude that the HXR emission in this phase was produced by high-energy electrons precipitating from this loop-like structure. Heated and "evaporated" plasmas, in turn, re-entered this structure. This also confirms that flare processes occurred within a closed configuration.

2.4. Microwave/Millimeter Burst

Total flux records from NoRP (Figure 10a – f) show a huge radio burst with its flux density reaching almost 10^5 sfu. A strong emission up to 5×10^4 sfu was recorded even at 80 GHz. The 80 GHz data had calibration problems (up to June 2005), which we fixed by means of a time-dependent correction inferred using hard copies of records from the detector of the radiometer. The time profiles at 17, 35, 80 GHz, and at 300 – 800 keV (dotted line in Figure 10d – f) are similar, thus suggesting a closeness of the sources responsible for radio and hard electromagnetic emissions. Until the onset of the π^0-decay emission at 06:45, features detectable at most frequencies correspond. The time profiles over 17 – 80 GHz start to show more fluctuations at this time (about 06:52). The microwave flux densities at these frequencies reach their maxima within the interval of 06:46 – 06:47, which corresponds to the maximum of the hardest gamma-rays emissions.

Figure 11 presents radio spectra computed from the NoRP data before, during, and after the flare maximum, with each point averaged over 5 seconds. The turnover frequency $\nu_{\rm peak}$ computed using interpolation is shown in Figure 10g. It is ≈ 30 GHz around the peak time, suggesting that microwaves came mainly from the strongest-field regions above the sunspots' umbrae.

The microwave spectral index computed from the ratios of fluxes at the highest frequencies is very hard, $\alpha \lesssim 1$. The spectra imply, however, that the slope at frequencies >80 GHz could be steeper, and real α larger. The electron power-law index corresponding to the optically thin limit is $\delta \approx 2.5$ (Dulk, 1985). From the HXR spectrum we found $\delta \approx 4.4 - 4.5$. The trapping effect hardens the microwave-emitting electron spectrum up to $\delta - 2$ (Silva, Wang, and Gary, 2000). Hence, a plausible power-law index of microwave-emitting electrons on 20 January 2005 was $\delta \approx 2.5 - 3.5$.

Near the peak of the burst, the density inferred from GOES data is $n_0 \approx 7 \times 10^{10}$ cm^{-3}. With an emitting region depth of 2×10^8 cm and the usually assumed relative number of accelerated electrons $n_{\rm acc}/n_0 = 10^{-4}$, one estimates a magnetic field strength of $B \approx 1500 - 2200$ G (Dulk, 1985). Thus, a large number of hard-spectrum electrons were gyrating in very strong magnetic fields. Since two sources in adjacent footpoints of a loop emit, the turnover frequency in the stronger-field footpoint was still higher.

Modeling the turnover and higher-frequency parts of the radio spectrum observed near the flare peak using Ramaty code (Ramaty, 1969; Ramaty *et al.*, 1994), provides a satisfactory fit (red in Figure 11b) with radio sources assumed to correspond to the observed HXR sources, $B \approx 1600$ G in the strongest-field region [(-2700 G, > 3100 G) at the photosphere], $\delta \approx 2.5 - 3.5$, and the relative number of accelerated electrons of $n_{(E>10\,{\rm keV})}/n_0 \approx 10^{-3} - 10^{-2}$. The lower-frequency microwaves were probably emitted by larger regions, as the spectra in Figure 11 imply. The major conclusion is that *the observed long-millimeter emissions could originate only in very strong magnetic fields just above sunspot umbrae, in accordance with other data.*

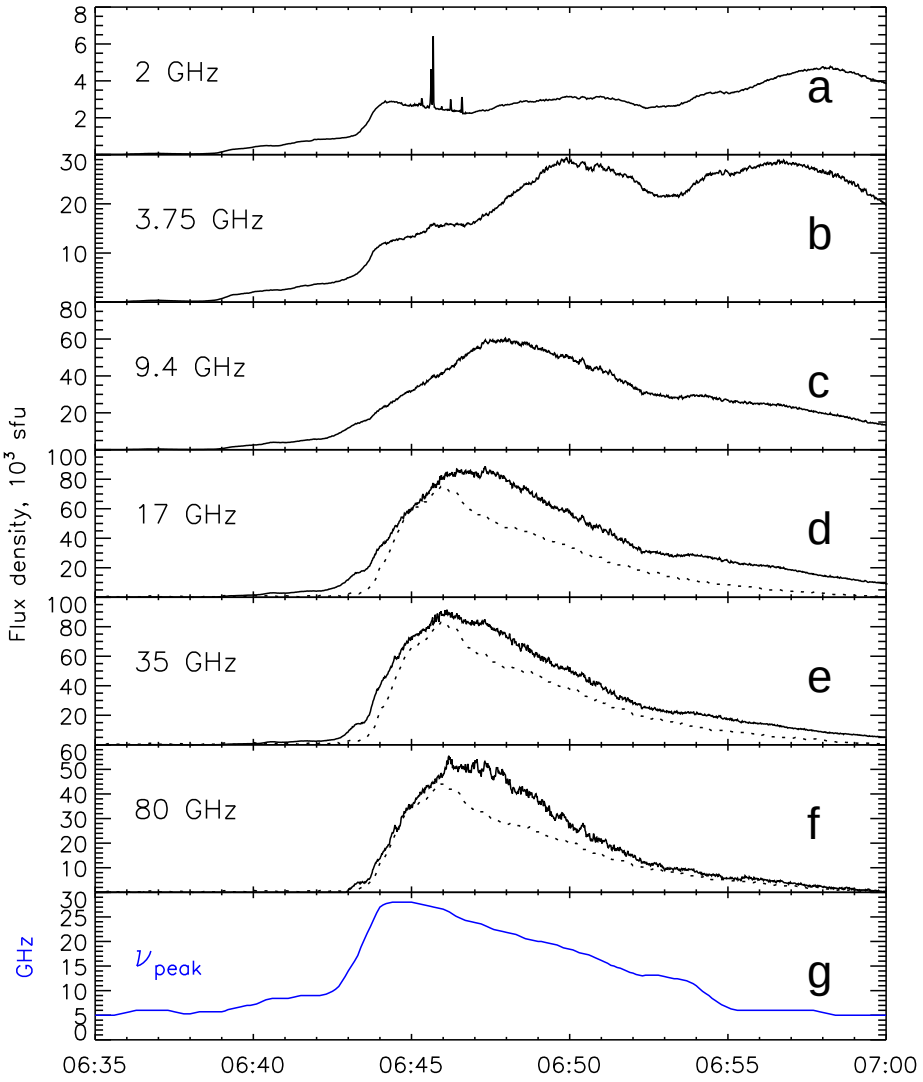

Figure 10. (a – f) NoRP total flux time profiles at 2 – 80 GHz, Stokes I. The vertical axes are in units of 10^3 sfu. Dotted lines show the hard X-ray emission at 300 – 800 keV according to RHESSI. (g) The turnover frequency of the microwave total flux spectrum according to NoRP data.

2.5. The CME and its Speed

Estimations of the CME speed in this event are difficult due to the prompt arrival at SOHO of a strong flux of high-energy protons, whose impacts on the CCD detector severely contaminated LASCO images. There is only one C2 frame at 06:54 (Figure 12g) in which the CME, with a central position angle (PA) of $290° - 293°$, is clearly detectable at $\approx 4.4R_\odot$. Assuming the loop-like structure, rising up to $\approx 1.3R_\odot$ in the EIT 195 Å frame at 06:36, corresponds to the frontal

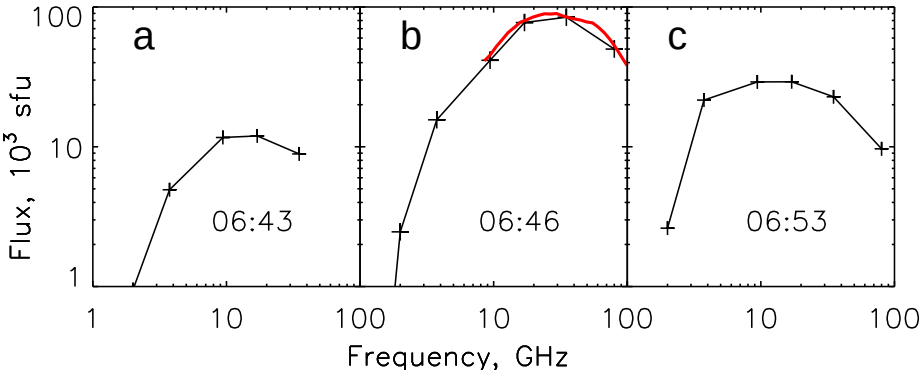

Figure 11. Total flux radio spectra computed from NoRP data (Stokes I, 10^3 sfu) before (a), during (b), and after the flare peak (c). Red: spectrum modeled with Ramaty code.

structure of the CME, one estimates its sky-plane speed $V \approx 2000$ km s^{-1}. From similar considerations Gopalswamy *et al.* (2005) and Simnett (2006) obtained the speeds of 2100 and 2500 km s^{-1}.

Another evaluation of Gopalswamy *et al.* (2005), that gave a record speed of 3242 km s^{-1}, seems to be greatly overestimated. Combining the EIT data point at 06:36 with the LASCO one in a second-order fit implies a constant CME acceleration, although the acceleration is know to initially increase sharply, from zero to a very high value, and then to decline to zero (see, *e.g.*, the review by Démoulin and Vial, 1992; Uralov, Grechnev, and Hudson, 2005). The CME may even decelerate. Moreover, as Zhang and Dere (2006) found, the greater the acceleration is, the shorter the time it acts over.

The identification of structures seen in LASCO and EIT images might be incorrect, especially the EIT loop and LASCO front. Frontal structures are rarely observed in EIT images as faint features indiscernible in non-subtracted frames (*e.g.*, Dere *et al.*, 1997; Uralov, Grechnev, and Hudson, 2005), whereas this expanding loop is distinct in raw EIT images. Frontal structures outrun all the other observable parts of the CME; thus, combining the LASCO and EIT data points one can greatly overestimate the CME speed.

However, the CME speed can be independently estimated from the conspicuous resemblance of halo CMEs in four homologous major events of 15 – 20 January. Each of them consisted of a bright structure rapidly expanding in a NW direction and a fainter, slower SE component. The speed ratios of CMEs on 15, 17, and 19 January were close, $\approx 3 - 4$. NW and SE components were also present in the 20 January CME (Figure 12), and their shapes were similar to those of preceding CMEs. As discussed below, the speeds of the SE components of the 19-th (360 km s^{-1}) and 20-th (485 km s^{-1}) January CMEs were of the same order.

Figure 12 shows this for the 19 and 20 January events. The onsets of both events also exhibited a strong resemblance: eruptions started with expansions of similar loops *L1* (*L1′*) visible in EIT images, and then much larger similar loops *L2* (*L2′*) started to expand. There is no perfect analogy between frames *a*, *b* and *e*, *f* due to the meager imaging rate of EIT, but the reordered sequence

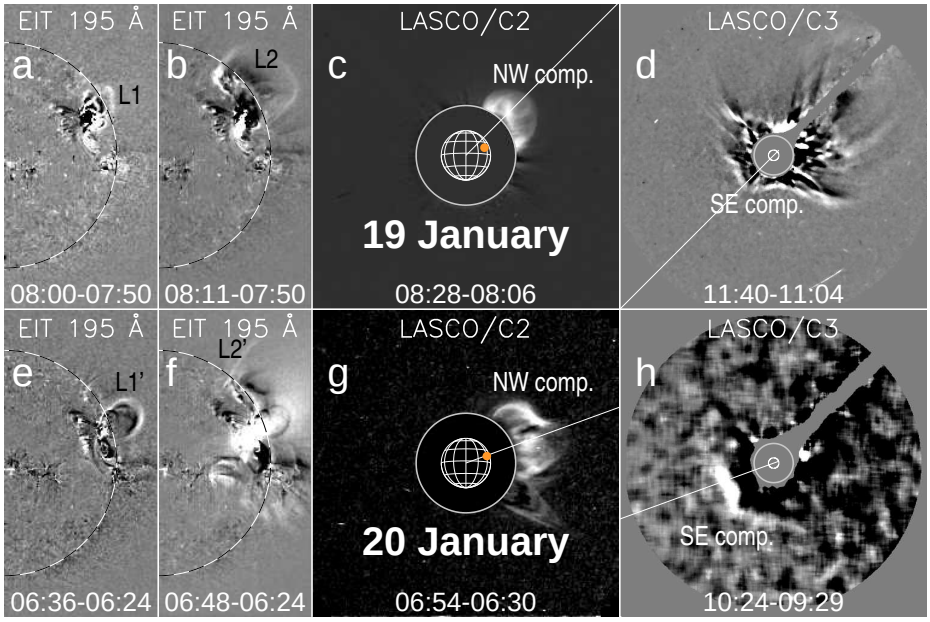

Figure 12. Homologous two-fold eruptions on 19 (top) and 20 (bottom) January shown by EIT 195 Å and LASCO/C2 & C3 difference images. Small orange disks denote AR 10720. Straight lines mark central position angles of the CMEs. Dashed circles in EIT images and thin white circles in LASCO images mark the limb. Larger gray circles denote the occulting disks. LASCO images of 20 January were heavily processed to reveal the CME.

a,e,b,f looks impressive. Also very similar are disturbed regions eastward and southward of AR 10720, bright chains between NE bases of loops *L1*, *L2* (*L1′*, *L2′*), and dimmings above the NW limb.

Let us compare the sky-plane speeds for the NW and SE parts of the two CMEs. Their source regions were close, N15 W51 on 19 and N14 W61 on 20 January. In both cases, we measure the speeds at the central position angles of the main NW parts. Since the NW part of the 20 January CME is in question, we analyze its analog on 19 January by considering its bright, sharp front rather than its weaker leading aureole, as done in the SOHO LASCO CME Catalog[7]. As shown in Figure 13a, the NW (PA≈315°) and SE (≈135°) components of the 19 January CME had speeds of 1540 and 360 km s^{-1}. In four frames of a LASCO/C3 running-difference movie for 20 January (08:54 – 10:56), despite strong contamination from energetic particles, the SE edge at PA≈110° can be detected moving away from the Sun. It is almost indiscernible; hence, its measurements have poor accuracy. The best frame of 10:24 – 09:29 in Figure 12h required heavy processing to reveal. We estimate its speed as ≈485 km s^{-1}. Simnett (2006) considered it as another CME (with a speed of 604 km s^{-1}), because its back-projected time to cross the limb was 07:15, well after the flare. However, the CME ejected from AR 10720, or nearby, traveled ≈ 1.9$R_\odot$ across

[7]http://cdaw.gsfc.nasa.gov/CME_list/

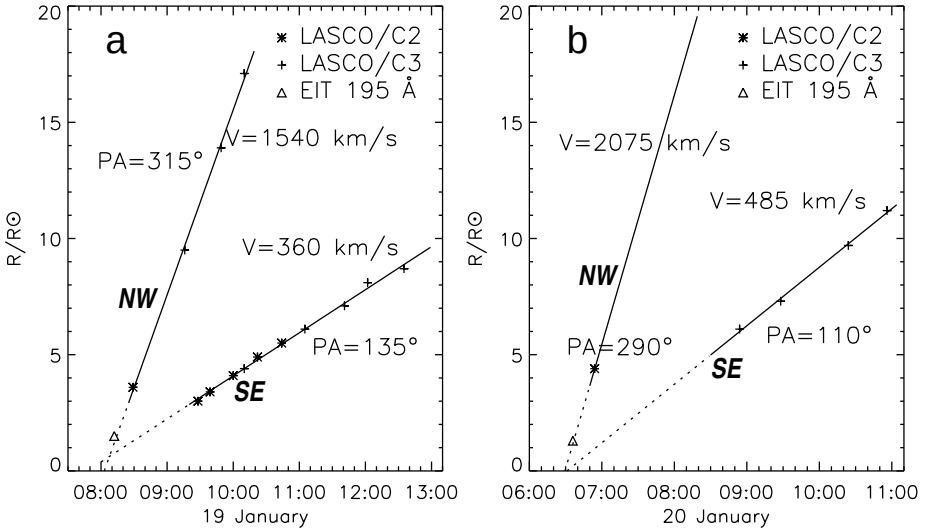

Figure 13. Height-time plots for NW and SE parts of the 19 (a) and 20 (b) January CMEs.

the solar disk before crossing the SE limb; therefore, using a speed estimated by Simnett (2006), it began at 06:39. This is very close to the eruption in AR 10720, while no other activity was registered anywhere on the Sun between 06:30 and 07:15. Consequently, this was the opposite side of the same CME.

Then, assuming the same ratio of the speeds of the NW and SE parts in the analogous CMEs of 19 and 20 January, and neglecting a small displacement of the eruption center, one obtains a speed for the NW component on 20 January of ≈ 2075 km s^{-1}, or 2585 km s^{-1} using the estimate of Simnett (2006).

The height-time plot for the NW component on 20 January in Figure 13b, for a speed of 2075 km s^{-1}, has been drawn across the only measured point of $\approx 4.4 R_{\odot}$ at 06:54 (LASCO/C2). Our way of estimating the CME speed is based on the linear fit of sparse data at large heights, which engenders large uncertainties in the initial parts, where acceleration occurs. Nevertheless, EIT data points should be briefly addressed. As noted, they likely correspond to some inner structures of CMEs; thus, they are expected to be beneath the height-time plots of the frontal structures. Since the initial acceleration is large, the initial parts of the height-time plots for the frontal structures must be curved upward, as Gopalswamy *et al.* (2005) showed in their Figure 5 (right). The proximity of EIT points to the linear-fit plots in Figure 13 for both 19 and 20 January CMEs therefore supports our estimates of CME speeds.

The NW parts of both CMEs apparently moved faster in the sky plane and rapidly became faint in their expansion. This is one more point of similarity between them and explains why the NW component in the 20 January CME was not detectable in the strongly contaminated LASCO/C3 images.

Note that shock speeds estimated from drift rates of type II bursts observed by a few observatories[8] in the analogous events of 15-th (1151 – 1900 $\mathrm{km\,s^{-1}}$), 17-th (1069 – 1578 $\mathrm{km\,s^{-1}}$), 19-th (1093 – 1368 $\mathrm{km\,s^{-1}}$), and 20-th (666 – 1300 $\mathrm{km\,s^{-1}}$) January systematically decrease, on average, in accordance with the CME speeds measured from LASCO images (see Table 1). Such estimates are strongly dependent on the coronal density model used and are therefore highly uncertain. Nevertheless, the shock speeds estimated for the three preceding CMEs are related to the measured speeds of the NW components by a factor of 0.4 – 0.6 (on average over observatories). This suggests a systematic factor to displace the estimated shock speeds with respect to the real ones. Thus, one might expect the CME speed on 20 January to be even slightly lower than that of the 19 January CME. In this case, our evaluation of the CME speed does not appear to be underestimated.

Our estimations are supported by data on the subsequent motion of the ICME. Measurements from the Solar Mass Ejection Imager data[9] indicate a moderately high ICME speed of ≈ 1280 $\mathrm{km\,s^{-1}}$ at elongations of 30 – 60°. This also corresponds to an average ICME speed between the Sun and Earth of ≈ 1200 $\mathrm{km\,s^{-1}}$, if a geomagnetic storm, which started at about 17 UT on 21 January, was due to its arrival at Earth. By extrapolating the "CME vs. ICME speed" curve shown by Owens and Cargill (2004, Fig. 3) plotted for the model with aerodynamic drag (Vršnak and Gopalswamy, 2002), one obtains an ICME speed of 1300 $\mathrm{km\,s^{-1}}$ corresponding to a CME speed of 2200 $\mathrm{km\,s^{-1}}$, while other existing models of ICME transit between the Sun and Earth provide lesser CME speeds. Pohjolainen *et al.* (2007) also addressed these issues and estimated a CME speed of 2500 $\mathrm{km\,s^{-1}}$ at $50R_\odot$, admitting that it may have reached about 3000 $\mathrm{km\,s^{-1}}$ in the interval of $(3-50)R_\odot$ and acknowledging significant uncertainties.

The CME speed on 20 January was high, but not extreme, and ranged between 2000 and 2600 km s^{-1} in the sky plane. According to all estimations, at 06:43, when hard emissions started, the CME frontal structure had reached $> 1R_\odot$ *above the solar surface, and the shock was even farther away.*

3. Relation to SEP and GLE

3.1. Comparison with Other Events from the Same Region

During 15 – 19 January, when AR 10720 was already in the western hemisphere, three other similar major events occurred in this active region. They included X class flares, strong microwave bursts, fast CMEs, and significant SEP fluxes. A comparison of all of these events holds the promise of identifying the origin of the SEPs. Table 1 lists their parameters as given in Solar Geophysical Data[10] and the SOHO LASCO CME Catalog.

[8] ftp://ftp.ngdc.noaa.gov/STP/SOLAR_DATA/SOLAR_RADIO/SPECTRAL/SPEC_NEW.05

[9] http://creme96.nrl.navy.mil/20Jan05/SMEI.html

[10] http://sgd.ngdc.noaa.gov/sgd/jsp/solarindex.jsp

Table 1. Characteristics of some western major events from AR 10720

Date	Time	GOES	Position	Radio flux, sfu ν, GHz		Proton flux, pfu E, MeV			CME speed
				8.8	15.4	>10	>50	>100	$\mathrm{km\,s^{-1}}$
15	22:48	X2.6	N14W09	20000	18000	300	10	0.4	2860
17	09:43	X3.8	N15W25	16000	17000	3000	300	25	2550
19	08:32	X1.3	N15W51	17000	15000	$<100^a$	<3	≈ 0.1	2020
20	06:44	X7.1	N14W61	41600	77400	1800	1100	680	2000 – 2600[b]

[a] On top of the background after the preceding event
[b] According to the compiled estimations described in the text

The sky-plane CME speeds on 15 and 17 January were even higher than on 20 January, although AR 10720 was not far from the solar disk center (thus, their real speeds could well exceed the projected ones). However, the SEP fluxes from these events were less than the 20 January event, contrary to the idea that CME speed is a major factor in determining the SEP productivity of CME-driven shocks. On the other hand, the SEP fluxes in Table 1 roughly correlate with flare emissions, in particular, at 15.4 GHz. One might ascribe the fact that proton fluxes were weaker on 15 and 17 January to suboptimal (although western) position of the flare. However, for the 19 January CME erupting from W51, the longitude could not appreciably reduce the proton flux, while its speed was also high. The speeds of all these CMEs greatly exceeded the Alfvén speed at $> 1R_\odot$ above the solar surface (P. Riley, 2006, private communication), suggesting that the CME-driven shocks were strong enough to effectively accelerate particles. Seed populations from previous CMEs do not appear to be drastically different for 17 – 20 January events.

The magnetic connection between the Sun and Earth probably played a significant role, but proton fluxes and microwaves appear to be closely related. The strongest fluxes of hard-spectrum protons near Earth were observed after the 20 January event, when the flare microwave emission was especially strong and hard. Note also that the proton flux was rather strong and hard in the 17 January event, when the microwave peak frequency exceeded 15.4 GHz, as well as in the 20 January event, unlike all others.

Our comparison also shows that the most distinctive feature of the 20 January event was not a large flux of medium-energy protons, but an extremely hard proton spectrum (see Table 1), which was a reason for the extreme GLE – at least, its large initial part. Flare emissions from the chromosphere and the lower corona are important indicators of the flare-acceleration of large quantities of energetic particles. *The magnetic field strength and the parameters of flare emission appear sufficient to determine extreme nature of the 20 January 2005 proton event, the CME speed is not a determining factor.*

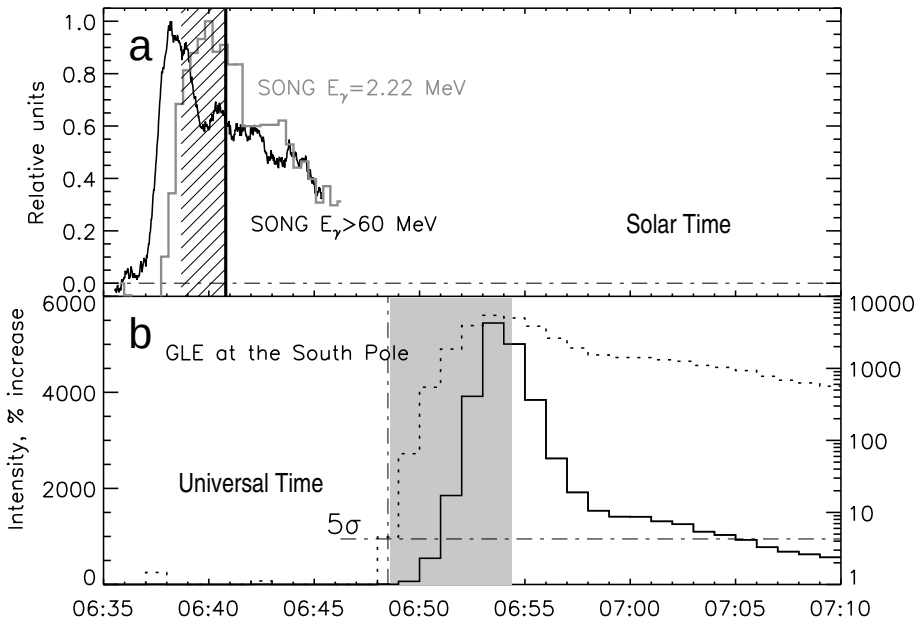

Figure 14. The impulsive, leading parts of gamma-ray time profiles and GLE. a) SONG gamma-ray time profile of $E_\gamma > 60$ MeV emission smoothed over 60 points and the 2.22 MeV line emission recorded with the SONG pulse-height analyzer (gray). The hatched interval corresponds to the **latest** possible escape times of 1 – 7 GeV protons responsible for the GLE onset. b) GLE measured at the South Pole NM station in the linear (solid) and logarithmic (dotted) scales. Shading marks the arrival interval of the largest proton flux estimated from the maximum of the gamma-ray burst.

3.2. Gamma-Ray Burst and Ground Level Enhancement

As noted, the earliest onset and the largest effect of the 20 January 2005 GLE was recorded with the neutron monitor (NM) at the South Pole (Figure 14b). The first protons arrived at Earth at 06:48:30 UT±30 s (above 5σ level, see the logarithmic scale). They were unusually fast compared to most GLEs, suggesting a perfect magnetic connection. To determine the origin of high-energy (> 300 MeV) protons responsible for the GLE, we start with a comparison of GLE onset time at the South Pole with the temporal characteristics of the π^0-decay emission (see Kuznetsov *et al.*, 2005a, 2006a,b; Simnett, 2006; Share *et al.*, 2006). As Figure 7 shows, the $E_\gamma > 60$ MeV gamma-rays are dominated by the π^0-decay emission.

To estimate the *latest possible escape time* of protons from/near the Sun, we consider their straight radial flight between the Sun and Earth by neglecting any delays, curvatures of their trajectory, and scattering, *i.e.*, conditions extremely favorable for their prompt transport. The Sun – Earth distance was 0.984 AU on 20 January that gives the solar time scale, ST = UT − 489 s[11]. Plainaki *et al.*

[11]Solar Time referring to an event on the Sun and calculated from UT by taking account of the propagation time

(2007) estimated the effective energy of protons at the GLE onset to be about 7 GeV, which corresponds to a velocity of $v = 0.993c$ and a flight time of 492 seconds. Hence, the protons responsible for the GLE onset had to depart the Sun **not later than** 06:40:18 ST±30 s.

If the energy of the first particles recorded with the South Pole NM was much less, ≈ 1 GeV ($v = 0.875c$ and a flight time 559 seconds), then their latest possible escape time was 06:39:11+30 s ST. Thus, allowing for all the uncertainties, the **latest** escape time of the first GLE particles was between 06:39:11−30 s ST for 1 GeV and 06:40:18+30 s ST for 7 GeV (a hatched box in Figure 14a). Even this latest-limit time interval is close to the sharp π^0-decay burst which peaked at 06:46 – 06:47 UT, *i.e.*, at 06:37:50 – 06:38:50 ST. This is the physical limit of the escape time of the first particles into interplanetary space.

The real path length of charged particles certainly exceeded the Sun – Earth distance due to non-zero pitch angles, scattering, *etc.* Thus, to arrive at Earth by 06:48:30 UT±30 s, the first protons had to leave the Sun still earlier than we estimated. This timing confirms a common origin of the protons responsible for the high-energy gamma-rays and the leading spike of the GLE.[12]

This conclusion of a common origin for the protons responsible for the π^0-decay emission and for the leading GLE spike is reinforced by comparing their time profiles. These curves resemble each other; each contains an impulsive, leading part followed by a long, smoother tail. Their leading parts are much alike in their rise times, durations, and fast decays; despite broadening of the GLE due to transport effects. These facts imply that the processes, which accelerated the particles responsible for the π^0-decay emission on one hand, and those responsible for the leading GLE spike on the other hand, *had proximate inceptions and comparable increments, acted over almost the same period, and then shifted from the impulsive mode to another, prolonged one, in a similar fashion.* The time differences between these processes did not exceed the uncertainties, and several reasons exist to account for this difference. An assumption that these mechanisms were different, independent, distant, and operated with different populations of particles, seems to be physically improbable.

The flux of particles at the South Pole reached its maximum while neutron monitors sensitive to the opposite direction of incident particles had not yet recorded the GLE. Thus, it had a 100% anisotropy, which indicates the direct arrival of particles from the Sun. The time profile recorded at the South Pole is therefore well connected with the injection function of solar cosmic rays influenced by transport effects. On the other hand, the π^0-decay emission supplies an approximate representation of the injection function. The rising phase of the GLE is affected by dispersion due to differences in path lengths and velocities, while the fast decay phase is extended due to scattering and the arrival of particles with large pitch angles. The time profiles of the π^0-decay emission and the GLE at the South Pole (Figure 14b) show that transport effects broadened the GLE, but did not significantly change its shape with respect to the gamma-ray burst.

[12]The model injection function of Sáiz *et al.* (2005) starts later than the physical limit and therefore should not be used in an analysis of the initial part of the GLE.

If the first 7 GeV GLE protons were accelerated and promptly escaped during the first π^0-decay sub-burst (06:43:40 UT or 06:35:31 ST) or the main burst (06:45:30 UT or 06:37:21 ST), then their real effective path length was between 1.30 and 1.65 of the Sun – Earth distance. This effective path length includes all transport effects, *e.g.*, spiraling due to non-zero pitch-angles, diffusion time, *etc.* The π^0-decay emission maximum (06:38 – 06:39 ST) corresponds to the largest number of high-energy protons in the solar atmosphere. The maximum of the GLE ($\approx$06:53:00) corresponds to the arrival of most of the 1 – 15 GeV protons. Therefore, the arrival times of protons emitted from the Sun near the π^0-decay emission maximum, with our estimated range of path lengths, should encompass the time of the GLE maximum. For protons of these energies with our estimated path lengths, arrival times range from 06:48:36 until 06:54:21 UT (shading in Figure 14b). Thus, the π^0-decay emission and GLE closely correspond to each other in time, and our estimate of the path length of high-energy protons is reasonable.

All these facts, considerations, and estimations demonstrate that the high-energy particles responsible for π^0-decay gamma-rays on the Sun, and the majority of those responsible for the leading GLE spike, belonged to the same population, and they acquired a significant part of their energy from the same acceleration process. No other realistic possibility appears to be consistent with all the facts.

4. Discussion

4.1. Overall Picture of the Solar Event

As shown in Section 2, the great event of 20 January was primed by the history of the active region, *i.e.*, the convergence of opposite-polarity domains and large shear motions. These are known to be precursors of big flares, which indeed occurred on 15 – 20 January. A distinctive feature of the biggest flare on 20 January was its occurrence just above sunspot umbrae where the magnetic fields were extremely strong, $\gtrsim$3000 G at the photosphere. This also ensured a high CME speed (cf. Švestka, 2001). Strong magnetic fields with a large stored non-potential component were most likely responsible for the outstanding features of this eruptive flare.

With the flare onset, opposite-polarity magnetic fluxes started to interact. The magnetic flux in the southern sunspot of N-polarity was larger. In the course of this interaction (probably via magnetic reconnection) its lesser counterparts in the northern sunspot became exhausted, and the process involved counterparts from the remaining area of the S-polarity domain. This manifested in an apparent motion of the brightest emission away from the northern sunspot, whereas the emissions in the southern sunspot persisted.

Particles accelerated in the corona streamed down to dense layers, precipitated, and heated them. High-energy electrons produced gyrosynchrotron emission, which was very strong and hard due to their large number, their hard spectrum, and strong magnetic fields. The lost energy was transformed into

heating and HXR and gamma-ray continua as well as Hα and 1600 Å emissions. Heavier particles produced gamma-rays, in particular, in discrete lines (cf. Ryan 2000; Somov 1992, 2006). The heated chromospheric plasmas evaporated and filled closed configurations, forming the hot SXR-emitting loop-like structure and a cooler arcade later on.

RHESSI shows the 2.22 MeV line source to be located on, and confined to, the northern ribbon where the coronal configuration was closed. This source was due to the precipitation of accelerated heavy particles with an energy of at least a few MeV, that had no direct access into a closed structure from outside. The hypothetical transport of external particles into the closed configuration could hardly proceed without other manifestations. Hence, these heavy particles could be accelerated only within the magnetic field of the active region, but not outside it. The absence of a detectable 2.22 MeV line from the southern source could be due to the suppression of ion precipitation in the sunspot umbra by mirroring because of much stronger field there than at the 2.22 MeV line centroid and nearby.

The above items constitute a self-consistent picture of the flare that encompasses observed phenomena and explains their particularities. This picture corresponds with many other observations and well-known concepts.

The CME on 20 January was not distinctive to the other CMEs of 15 – 19 January from the same active region, and its speed, 2000 – 2600 km s^{-1}, was not higher than some others. This is consistent with a conclusion of Reinard and Andrews (2006) that the only difference between SEP-related and non-SEP-related CMEs is their 1.36 higher average speed. Both slow and fast CMEs were present in both groups. On the other hand, *comparison with other events from AR 10720 demonstrates that the parameters of the flare alone determine the extreme nature of the 20 January proton event.*

4.2. Radio Burst and Proton Event

Both the qualitative and quantitative features of the electromagnetic emissions of the 20 January 2005 *flare* are indicative of its proton productivity. West flares with strong non-impulsive radio bursts at frequencies $\gtrsim 30$ GHz are known to be followed by SEP events; the strongest ones produce GLEs (Croom, 1970; Cliver, 2006). On the other hand, intense SEP events usually occur if the microwave burst is strong. Therefore, the association of the largest GLE with the flare producing the highest-energy particle flux is not surprising. The huge radio burst on 20 January exceeds all the criteria for *flare proton productivity* established in 1970 – 1980s, including the well-known "U-like spectrum" (see Croom, 1971; Castelli *et al.*, 1977; Akinyan, Fomichev, and Chertok, 1980a,b, 1981).

An important test of the flare origin of near-Earth protons is the comparison of their spectrum, at several tens of MeV, with the microwave spectrum. The peak integral spectral index of protons, roughly estimated from differential GOES-11 channels, is $\approx 1.1 - 1.3$ in this range, one of the hardest ever observed. The expected proton index can be estimated from radio data in three different ways. *i*) From the ratio of flux densities (Chertok, 1982) observed with NoRP at 9 and 17 GHz, $F_9/F_{17} \approx 0.7$, it is $0.9F_9/F_{17} + 0.4 \approx 1$. *ii*) From the spectral maximum

of the microwave burst, 30 GHz (Chertok, 1990), which provides a similar proton index. *iii*) From the parameters of the U-like spectrum (Bakshi and Barron, 1979) it is $1.185/\log_{10}(\nu_{\rm peak}/\nu_{\rm min}) \approx 0.8$. All three estimates are close to the observed integral spectral index of protons. With a strong estimated proton flux and very hard spectrum at several tens of MeV, microwave diagnostics point to a major proton flux at higher energies, *i.e.*, an intense GLE.

A glance at lists of radio bursts (*e.g.*, the NoRP Event List[13]) and proton events confirms that strong microwave/millimeter emissions *e.g.*, with a flux density of $> 10^4$ sfu at 35 GHz, and high turnover frequency are typical of most major SEP/GLE events, including some extreme proton events of recent years. However, there are exceptions, *e.g.*, when strong proton fluxes near Earth were associated with rather weak bursts. At the same time, the magnetic connectivity between the Sun and Earth is certainly important. The relationship between strong microwave bursts and proton events (see also Cliver *et al.*, 1989) needs further detailed analysis, which is currently in progress.

Advocating SEP acceleration by coronal shocks, Kahler (1982) ascribed the correlation between SEP fluxes and the parameters of microwave bursts to the "Big Flare Syndrome", the general association between a flare's energy release and the magnitude of its manifestations (also cf. Švestka, 2001). This tendency is certainly present, but it could hardly ensure the correspondence between the spectra of protons near Earth and microwave bursts (Bakshi and Barron, 1979; Chertok, 1982, 1990). If the role of coronal shocks in the acceleration of particles is even more significant, then, as our results demonstrate, energy release in the source regions of eruptive events, manifesting in flare emissions, is an important factor in determining the eventual SEP outcome.

Powerful microwave/millimeter emissions with high turnover frequency, radiated by numerous electrons with a hard spectrum in strong magnetic fields, are typical of major proton flares, but not of all proton events.

4.3. Where Did the Protons Come From?

Both observations and estimations do not obviously rule out the acceleration of particles in either the flare or the CME-driven shock. Indeed, if the CME started around 06:36, accelerated in ≈ 5 minutes ($5-10$ km s^{-2}) up to a speed of $2000-2600$ km s^{-1} (well in excess of the Alfvén speed), and the piston-driven wave steepened into a shock in a similar time frame, then the appearance of the shock is roughly co-temporal with the π^0-decay burst. At that time, the CME was at $\approx (2-3)R_\odot$, consistent with shock-acceleration.

On the other hand, the observations also appear to be consistent with a flare-related origin of the accelerated protons. As found in Section 2, sources of electromagnetic flare emissions produced by accelerated electrons and moderate-energy protons, from the microwave/millimeter burst up to the 2.2 MeV line gamma-rays, were compact and located inside a volume confined by flare ribbons and the SXR-emitting loop-like structure. The time profiles of these emissions

[13] http://solar.nro.nao.ac.jp/norp/html/event/

closely matched each other. Thus, all these emissions were generated within a compact closed structure above the active region, and the particles responsible for them were accelerated there also.

Cliver, Kahler, and Vestrand (1993) proposed that particles accelerated by a CME-driven shock could then precipitate back in dense layers of the solar atmosphere and produce gamma-rays. In this scenario, the 2.22 MeV line gamma-ray sources would be widespread (cf. Hurford *et al.*, 2006a), dominating the "twin" dimmings near the ends of a post-eruptive arcade (cf. Figure 8b), because such dimmings are considered to be bases of an expanding flux rope, the body of a CME (Hudson and Webb, 1997; Zarro *et al.*, 1999; Webb *et al.*, 2000). However, the 2.22 MeV line source was compact, with its centroid located at a flare ribbon, far from the dimmings (see Figure 8a). The CME was located $> 1R_{\odot}$ from the active region and so could not control the detailed course of the flare, nor could the even more distant shock front.

The observed manifestations of accelerated electrons and protons match the standard picture of a flare. In this picture, particles accelerated in the corona stream down along magnetic field lines. They then precipitate in dense layers and heat them. This causes emissions from flare ribbons. It also causes chromospheric evaporation to fill closed coronal structures and produce soft X-rays (*e.g.*, Somov, 1992; 2006). Our analysis does not address the escape of particles into interplanetary space, which could be due to drifts (*e.g.*, in electric fields) of particles accelerated in the flare region to open magnetic field lines, which are known to be always present in active regions (*e.g.*, Fisk and Zurbuchen, 2006). As Cane, Erickson, and Prestage (2002) showed, open magnetic fields between the low corona and the Earth do exist, ensuring the transport of electrons and protons of various energies. Note also the favorable longitude and proximity to the ecliptic plane ($\approx 9^{\circ}$) of the active region on 20 January.

In Section 3 we established that the high-energy particles responsible for the π^0-decay gamma-rays and the majority of those responsible for the leading spike of the GLE belonged to the same population and were accelerated by the same mechanism. As shown in Section 2.2.1, the time profiles of the π^0-decay emission and lower-energy emissions (in particular, electron bremsstrahlung) were close in time and roughly similar, but still different. These dissimilarities might mean that these emissions were generated by either (i) two different particle components (G.H. Share *et al.*, 2007, private communication) or (ii) the same population with variable parameters. In the former case, a reason could be (a) an extra process, which started to operate in the flare region slightly later and accelerated heavy particles up to > 300 MeV, and (b) another source located at a distance, including a CME-driven shock.

However, the single-population case is favored by the correspondence of the structural details in time profiles of the π^0-decay and lower-energy emissions including bremsstrahlung (Figure 3) and microwaves (Figure 10d,e; *e.g.*, peaks at 06:46 and 06:47:15), with their relative magnitudes corresponding to a continuous spectrum. The relative timing of the π^0-decay and lower-energy bursts is consistent with variations in the energy release rate in the flare. The energy release rate, in turn, is directly related to the energy and quantity of accelerated particles. Hard electromagnetic emissions (in particular, the π^0-decay one) peak

around 06:46, as did the microwave burst. At that time, the flare was located in the strongest magnetic fields (Sections 2.2.3, 2.4), and the energy, and number, of accelerated particles reached their maxima. Thus, the peak time of the π^0-decay burst is consistent with a flare origin, where it would be expected to start later than the lower-energy emissions, *i.e.*, when the energy release rate became high enough.

Correspondence between the parameters of the (flare originating) microwave/millimeter burst with those of the protons responsible for the initial, impulsive part of the SEP/GLE, including such a delicate characteristic as a hard energy spectrum of protons (Section 4.2), supports flare-related acceleration for this part of the SEP/GLE. Only the flare, not the CME, had extreme characteristics comparable with those of the 20 January 2005 proton event. Note that from a similar analysis of a few other events, Li *et al.* (2007a,b) also concluded that the particles responsible for the impulsive, initial component of GLEs were accelerated in flare current sheets.

Our results favor acceleration of protons just in the flare. On the other hand, the available data do not permit us to determine if the GLE-productive particles acquired energy up to $\gtrsim 7\,\mathrm{GeV}$ in the flare, or by an additional acceleration mechanism, *e.g.*, by a CME-driven shock (see Desai *et al.*, 2006). A posterior extra shock-acceleration is favored if the particles constituting a seed population (see Tylka *et al.*, 2005) collide with its convex front from outside with a small angle. However, this mechanism does not appear to be efficient, if particles collide with it from inside, which was most likely the case during the main flare phase of the 20 January 2005 event.

4.4. Comments on Later Manifestations and SEP Properties

Our considerations addressed the main stage of the flare and the related initial GLE spike to minimize secondary factors and transport effects in interplanetary space, which might influence SEP properties (*e.g.*, Cane *et al.*, 2003, 2006; Ng, Reames, and Tylka, 2003; Tylka *et al.*, 2005). Here we note that, in its next orbit, RHESSI registered gamma-rays identified with the π^0-decay emission with a decay time of $\tau_{\pi^0} \approx 100$ min, while the 2.22 MeV line emission (see Figure 14a) and nuclear de-excitation emissions decayed with $\tau_{2.22\ \mathrm{MeV}} \lesssim 10$ min (Share *et al.*, 2006; G.H. Share, 2007, private communication). It is unclear if long-decay gamma-ray emissions are generally due to prolonged acceleration or storage of impulsively accelerated protons (Ryan, 2000). In our event, a CME-driven shock cannot be responsible for gamma-rays with $\tau_{\pi^0} \approx 100$ min. Such an acceleration in the active region should accelerate electrons as well, but Learmonth records[14] show no evidence of this in the radio domain. If the long gamma-ray emissions were due to trapped protons then the decay times would be limited by their collision rate. The mean free path λ_i of a fast ion with a mass m_i, charge e_i, and an initial velocity v_0, in a plasma with a number density n, is $\lambda_\mathrm{i} = m_\mathrm{i} m_\mathrm{e} {v_0}^4 / (16\pi e_\mathrm{i} e_\mathrm{e} \Lambda n)$, where $\Lambda \approx 10$ Coulomb logarithm, e_e and m_e are

[14] http://www.ngdc.noaa.gov/stp/SOLAR/ftpsolarradio.html

the electron charge and mass; $\tau_{\rm coll} \approx \lambda_{\rm i}/v_0$. With a density in the SXR-emitting loop-like structure of $\approx 10^{11}\,{\rm cm}^{-3}$, $\tau \approx 80$ minutes for 300 MeV protons and $\tau \approx 4$ minutes for 30 MeV protons are close to the observed parameters. On the other hand, with $n < 10^9\,{\rm cm}^{-3}$ expected in the corona at heights $> 1R_\odot$, the collision time for 300 MeV protons is very long, $\tau > 120$ hours. Thus, the observed decay times of gamma-ray emissions appear to be consistent with the trapping of protons in the observed flare loop.

The major conclusion drawn from analyses of the SEP composition, based on observations during this SEP event[15], is its correspondence to "gradual events", which are believed to be due to acceleration in CME-driven shocks (Reames, 1995), rather than in a flare. However, Labrador *et al.* (2005) inferred an acceleration time of < 90 s, which appears to be consistent with the time profiles of gamma-ray emissions. R.A. Mewaldt (2007, private communication) found that the measured variations of the Fe/O ratio might be indicative of an impulsive flare-related component along with a longer gradual one, as suggested by Cane *et al.* (2003, 2006). However, as Ng, Reames, and Tylka (2003) showed, initial enhancements of the Fe/O ratio can be due to transport effects. Distinguishing all these effects does not seem to be a simple task.

Thus, the situation with the SEP composition is not obvious. Analyses of the corresponding data (especially on such short timescales as the leading SEP/GLE spike), as well as related issues, probably require the consideration of several complex factors. A simplified glance at these data might lead to mistaken conclusions about the origin of SEPs. Furthermore, as Somov and Chertok (1996)[16] pointed out, the observed properties of SEPs might be dependent on plasma parameters at the acceleration site. In particular, if the acceleration of ions occurs in a low-density region above the flare site, relatively high in the corona, then the number of Coulomb collisions might be too small to ensure their Maxwellian distribution, which is inherent in the temperature of the acceleration site. As a result, these SEPs could retain properties typical of background coronal conditions.

To determine if the probable contribution from the CME-driven shock to the acceleration of heavier ions was as significant as the contribution from the flare-accelerated protons to the leading spike of the GLE, a comparison should be made with other events, especially with those from the same active region. In this comparison, not only the SEP composition, but also total fluxes are important. Otherwise, there is no apparent reason to relate the outstanding properties of the 20 January 2005 event with the parameters of the CME only.

5. Summary and Conclusion

In considering the extreme proton event of 20 January 2005, we first carried out a comprehensive analysis of the flare, based on multi-spectral observations, and second, investigated the origin of the energetic protons corresponding to the leading SEP/GLE spike. Our conclusions regarding the flare are as follows.

[15] http://creme96.nrl.navy.mil/20Jan05/

[16] Chapman Conference "Coronal mass ejections: causes and consequences", Montana State University, Bozeman, Montana

1. Imaging data in Hα, 1600 Å, soft and hard X-rays, EUV, and 2.22 MeV neutron-capture line show that the sources of these emissions were compact and localized within a volume confined by flare ribbons, which crossed the umbrae of the largest sunspots with strong magnetic fields.
2. Non-imaging data extend this conclusion to microwave/millimeter, lower-energy, and medium-energy gamma-ray emissions, because the time profiles of the major flare component, caused by accelerated electrons and protons, were similar and closely related, particularly in time.
3. The π^0-decay emission time profile was much like those of lower energy, but their differences prevent us from confidently asserting a common source. Nevertheless, co-temporal structural details in the π^0-decay and lower-energy time profiles (their magnitude corresponds to a continuous spectrum) indicate their common nature; the timing of the π^0-decay gamma-ray burst corresponds to the highest energy release rate in the flare (Section 4.3). Thus, its flare origin appears to be preferable. However, one should not consider the flare origin to be proven.
4. The above considerations favor the acceleration of both the electrons and protons, responsible for various emissions (at least, at moderate energies), within the magnetic field of the active region at a moderate height above the sunspots. The manifestations of the electron and proton components correspond to the standard picture of a flare, in which chromospheric ribbons and compact sources of hard emissions map the footpoints of newly formed magnetic loops, along which energetic particles fly downward and bombard the lower atmosphere.
5. The presence of a large number of accelerated particles in strong magnetic fields is demonstrated by the fact that the flare was accompanied by one of the strongest and hardest-spectrum microwave bursts ever observed, with a peak flux density of almost 10^5 sfu at 30 GHz and a very strong (5×10^4 sfu) emission at 80 GHz.
6. Evaluations of the 20 January CME sky-plane speed from various available data result in an estimate of $2000 - 2600\ \mathrm{km\,s^{-1}}$.

Regarding the SEP/GLE aspect of this event, we first note that there is no clear observational evidence to state with certainty if it was due to the flare or the CME-driven shock. However, our analysis favors the flare region as the probable site of acceleration of the particles responsible for the leading SEP/GLE spike, rather than the shock ahead of the CME, as supported by the following arguments.

1. The compactness of the gamma-ray sources and similarity of the time profiles of different emissions could hardly be expected if high-energy particles were accelerated in an extended shock front ahead of the receding CME.
2. The proton event under consideration was extreme, not in its CME speed, but in the parameters of the flare itself, particularly in the huge microwave/millimeter radio burst.
3. There is a significant correspondence between the hardness of the microwave spectrum and the hardness of the energetic spectrum of the SEP and GLE protons.

4. The time of emission from the Sun of high-energy protons responsible for the onset of the GLE is close to that of the π^0-decay emission.
5. The gamma-ray burst and the leading GLE spike have similar shapes.
6. The decay times of gamma-ray emissions computed by G.H. Share (2007, private communication) from RHESSI data agree with the collision times of protons trapped in the observed flare loop, but not with those stored higher in the corona.

The available data, together with our results, do not rule out a possible role for the CME-driven shock in the acceleration of particles during the initial part of the GLE. Similarly, the role of flare acceleration cannot be completely ruled out for later stages of the SEP event, when the shock seems to dominate. Advocating "shock-acceleration only" or "flare-acceleration only" does not seem to be productive (see Švestka, 2001; Kallenrode, 2003). Studies of the relative contribution from acceleration in flares and CME-driven shocks appears to be more fruitful. They can vary for dissimilar events, their different stages, and in different energy ranges.

The 20 January 2005 event represents a distinct class of extreme solar flares. They amount to a small percentage of all flares, but probably constitute the majority of events which can be proton-rich under favorable Sun – Earth connections. The expected features of these flares are: occurrence near or above sunspot umbrae in strong magnetic fields; powerful bursts in microwaves; and at long millimeter wavelengths. These events are very dangerous due to a high probability of strong proton fluxes with hard spectra. This fact highlights the importance of measuring strong magnetic fields in solar active regions, as well as patrol observations of the total radio flux at long millimeter wavelengths, for the forecast and diagnosis of major proton events. Currently, only NoRP observations at 35 and 80 GHz are available from ≈ 22 till ≈ 08 UT.

Acknowledgements We appreciate discussions and assistance of A.J. Tylka, G.H. Share, G.J. Hurford, M.A. Livshits, G.V. Rudenko, I.I. Myshyakov, S.A. Bogachev, A.B. Struminsky, S.M. White, B.R. Dennis, and A.K. Tolbert. We are grateful to G.H. Share and G.J. Hurford for supplying us with preliminary RHESSI data. We thank the anonymous reviewers for useful remarks.

The CME catalog is generated and maintained at the CDAW Data Center by NASA and The Catholic University of America in cooperation with the Naval Research Laboratory. We thank the teams of EIT, LASCO, MDI on SOHO (ESA & NASA); the USAF RSTN Network, and the GOES satellites.

The study is supported by the Russian Foundation of Basic Research (05-02-17487, 06-02-16106, 06-02-16239, 06-02-16295, and 07-02-00101), the Federal Ministry of Education and Science (8499.2006.2, 4573.2008.2, and UR.02.02.509/05-1), and the programs of the Russian Academy of Sciences "Solar Activity and Physical Processes in the Sun-Earth System" and "Plasma Heliophysics". VG is indebted to the SHINE and the US National Science Foundation for providing support to attend the 2007 Workshop. Discussions held there greatly helped in illuminating different aspects of problems in question.

References

Akinyan, S. T., Chertok, I. M., Fomichev, V. V.: 1980a, In: Donnely, R.F. (ed.), *Solar-Terrestrial Prediction Proceedings, Vol. 3*, D-14.

Akinyan, S. T., Fomichev, V. V., Chertok, I. M.: 1980b, *Geomagnetizm i Aeronomiia* **20**, 385, (in Russian).

Akinyan, S. T., Fomichev, V. V., Chertok, I. M.: 1981, *Phys. Solariterr.*, Potsdam **17**, 135.

Andrews, M. D.: 2001, *Solar Phys.* **204**, 181.

Bakshi, P., Barron, W.: 1979, *J. Geophys. Res.* **84**, 131.

Belov, A., Garcia, H., Kurt, V., Mavromichalaki, H., Gerontidou, M.: 2005, *Solar Phys.* **229**, 135.

Bieber, J. W., Clem, J., Evenson, P., Pyle, R., Ruffolo, D., Rujiwarodom, M., Saiz, A., Duldig, M., Humble, J.: 2005, AGU Fall Meeting, abstract #SH21A-03.

Birn, J., Gosling, J. T., Hesse, M., Forbes, T. G., Priest, E. R.: 2000, *Astrophys. J.* **541**, 1078.

Brueckner, G. E, Howard, R. A., Koomen, M. J., Korendyke, C. M., Michels, D. J., Moses, J. D., *et al.*: 1995, *Solar Phys.* **162**, 357.

Cane, H. V., Erickson, W. C., Prestage, N. P.: 2002, *J. Geophys. Res.* **107**, A101315.

Cane, H. V., von Rosenvinge, T. T., Cohen, C. M. S., Mewaldt, R. A.: 2003, *Geophys. Res. Lett.* **30**, 8017.

Cane, H. V., Mewaldt, R. A., Cohen, C. M. S., von Rosenvinge, T. T.: 2006, *J. Geophys. Res.* **111**, A06S90.

Castelli, J. P., Barron, W. R.: 1977, *J. Geophys. Res.* **82**, 1275.

Chertok, I. M.: 1982, *Geomagnetizm i Aeronomiia* **22**, 182, (in Russian).

Chertok, I. M.: 1990, *Astron. Nachr.* **311**, 379.

Chertok, I. M.: 1995, *24th Int. Cosmic Ray Conf.* **4**, 78.

Chertok, I. M., Grechnev, V. V.: 2005, *Solar Phys.* **229**, 95.

Cliver, E. W., Forrest, D. J., Cane, H. V., Reames, D. V., McGuire, R. E., von Rosenvinge, T. T., Kane, S. R., MacDowall, R. J.: 1989, *Astrophys. J.* **343**, 953.

Cliver, E. W., Kahler, S. W., Vestrand, W. T.: 1993, *23 Int. Cosmic Ray Conf.* **3**, 91.

Cliver, E. W.: 2000, In: Mewaldt, R.A., Jokipii, J.R., Lee, M.A., Eberhard Möbius, E., Zurbuchen, T.H. (eds.), *Acceleration and Transport of Energetic Particles Observed in the Heliosphere, AIP Conf. Proc.* **528**, 21.

Cliver, E. W.: 2006, *Astrophys. J.* **639**, 1206.

Croom, D. L.: 1970, *Solar Phys.* **15**, 414.

Croom, D. L.: 1971, *Solar Phys.* **19**, 152.

Delaboudinière, J.-P., Artzner, G. E., Brunaud, J., Gabriel, A. H., Hochedez, J. F., Millier, F., *et al.*: 1995, *Solar Phys.* **162**, 291.

Démoulin, P., Vial, J. C.: 1992, *Solar Phys.* **141**, 289.

Dere, K. P., Brueckner, G. E., Howard, R. A., Koomen, M. J., Korendyke, C. M., Kreplin, R. W., *et al.*: 1997, *Solar Phys.* **175**, 601.

Desai, M. I., Mason, G. M., Gold, R. E., Krimigis, S. M., Cohen, C. M. S., Mewaldt, R. A., Mazur, J. E., Dwyer, J. R.: 2006, *Astrophys. J.* **649**, 470.

Didkovsky, L. V., Judge, D. L., Jones, A. R., Rhodes, E. J., Jr., Gurman, J. B.: 2006, *Astron. Nachr.* **327**, 314.

Dulk, G. A.: 1985, *Annu. Rev. Astron. Astrophys.* **23**, 169.

Fisk, L. A., Zurbuchen, T. H.: 2006, *J. Geophys. Res.* **111**, A09115.

Gopalswamy, N., Xie, H., Yashiro, S., Usoskin, I.: 2005, *29th Int. Cosmic Ray Conf.* **1**, 169.

Grechnev, V. V.: 2003, *Solar Phys.* **213**, 103.

Grechnev, V. V.: 2004, In: Stepanov, A.V., Benevolenskaya, E.E., Kosovichev, A.G. (eds.), *Multi-Wavelength Investigations of Solar Activity, IAU Symp.* **223**, 625.

Grechnev, V. V., Kundu, M. R., Nindos, A.: 2006, *Publ. Astron. Soc. Japan* **58**, 47.

Handy, B. N., Acton, L. W., Kankelborg, C. C., Wolfson, C. J., Akin, D. J., Bruner, M. E., *et al.*: 1999, *Solar Phys.* **187**, 229.

Hill, S. M., Pizzo, V. J., Balch, C. C., Biesecker, D. A., Bornmann, P., Hildner, E., *et al.*: 2005, *Solar Phys.* **226**, 255.

Hudson, H., Ryan, J.: 1995, *Annu. Rev. Astron. Astrophys.* **33**, 239.

Hudson, H. S., Webb, D. F.: 1997, In: Crooker, N., Joselyn, J.A., Feynmann, J. (eds.), *Coronal Mass Ejections, Geophys. Monograph* **99**, 27.

Hurford, G. J., Krucker, S., Lin, R. P., Schwartz, R. A., Share, G. H., Smith, D. M.: 2006a, *Astrophys. J.* **644**, L93.

Hurford, G. J., Krucker, S., Lin, R. P., Schwartz, R. A., Share, G. H., Smith, D. M.: 2006b, AAS SPD Meeting, Abstract #28.04.
Kahler, S. W.: 1982, *J. Geophys. Res.* **87**, 3439.
Kahler, S. W.: 2001, In: Song, P., Singer, H.J., Siscoe, G.L. (eds.), *Space Weather, Geophys. Monograph* **125**, 109.
Kallenrode, M.-B.: 2003, *J. Phys. G.* **29**, 965.
Klein K.-L., Trottet G.: 2001, *Space Sci Rev.* **95**, 215.
Krucker, S., Hurford, G. J., Lin, R. P.: 2005, AGU Fall Meeting, Abstract #SH21A-01.
Kuznetsov, S., Kudela, K., Myagkova, I., Podorolskiy, A., Ryumin, S., Yushkov, B.: 2004, *Indian J. Radio Space Phys.* **33**, 353.
Kuznetsov, S. N., Kurt, V. G., Yushkov, B. Yu., Myagkova, I. N., Kudela, K., Kaššovicová, J., Slivka, M.: 2005a, *29th Int. Cosmic Ray Conf.* **1**, 49.
Kuznetsov, S., Kurt, V., Myagkova, I., Yushkov, B., Kudela, K., Belov, A., Caroubalos, C., Hilaris, A., Mavromichalaki, H., Moussas, X., Preka-Papadema, P.: 2005b, *Int. J. Modern Phys. A*, 20, 6705.
Kuznetsov, S. N., Kurt, V. G., Yushkov, B. Yu., Myagkova, I. N., Kudela, K., Kaššovicová, J., Slivka, M.: 2006a, *Contrib. Astron. Obs. Skalnaté Pleso* **36**, 85.
Kuznetsov, S. N., Kurt, V. G., Yushkov, B. Yu., Kudela, K.: 2006b, *Bull. Russian Acad. Sci., Physics* **70**, 1665.
Kuznetsov, S. N., Kurt, V. G., Yushkov, B. Yu., Kudela, K. 2007: 2007, *30th Int. Cosmic Ray Conf.* SH 1.5, paper 0539, in press.
Kuznetsov, S. N., Kurt, V. G., Yushkov, B. Yu., Kudela, K., Galkin V. I., Myagkova I. N.: 2008, *Solar Phys.*, in press.
Labrador, A. W., Leske, R. A., Mewaldt, R. A., Stone, E. C., von Rosenvinge, T. T.: 2005, *29th Int. Cosmic Ray Conf.* **1**, 99.
Li, C., Tang, Y.H., Dai, Y., Zong, W.G., Fang, C.: 2007a, *Astron. Astrophys.* **461**, 1115.
Li, C., Tang, Y.H., Dai, Y., Fang, C., Vial, J.-C.: 2007b, *Astron. Astrophys.* **472**, 283.
Lin, R. P., Dennis, B. R., Hurford, G. J., Smith, D. M., Zehnder, A., Harvey, P. R., *et al.*: 2002, *Solar Phys.* **210**, 3.
Liu, W., Liu, S., Jiang, Y. W., Petrosian, V.: 2006, *Astrophys. J.* **649**, 1124.
Livshits, M. A., Belov, A. V.: 2004, *Astron. Rep.* **48**, 665.
Nakajima, H., Sekiguchi, H., Sawa, M., Kai, K., Kawashima, S.: 1985, *Publ. Astron. Soc. Japan* **37**, 163.
Neupert, W. M.: 1968, *Astrophys. J.* **153**, L59.
Ng, C. K., Reames, D. V., Tylka, A. J.: 2003, *Astrophys. J.* **591**, 461.
Oraevsky, V. N., Sobelman, I. I.: 2002, *Astron. Lett.* **28**, 401.
Owens, M., Cargill, P.: 2004, *Ann. Geophys.* **22**, 661.
Plainaki, C., Belov, A., Eroshenko, E., Mavromichalaki, H., Yanke, V.: 2007, *J. Geophys. Res.* **112**, A04102.
Pohjolainen, S., van Driel-Gesztelyi, L., Culhane, J. L., Manoharan, P. K., Elliott, H. A.: 2007, *Solar Phys.* **244**, 167.
Ramaty, R.: 1969, *Astrophys. J.* **158**, 753.
Ramaty, R., Kozlovsky, B., Lingelfelter, R. E.: 1975, *Space Sci. Rev.* **18**, 341.
Ramaty, R.: 1986, In: Sturrock, P.A. (ed.), *Physics of the Sun, Vol. 2*, D. Reidel Publ. Co., Dordrecht, 291.
Ramaty, R., Schwartz, R. A., Enome, S., Nakajima, H.: 1994, *Astrophys. J.* **436**, 941.
Reames, D. V.: 1999, *Space Sci Rev.* **90**, 413.
Reinard, A. A., Andrews, M. A.: 2006, *Adv. Space Res.* **38**, 480.
Ryan, J. M.: 2000, *Space Sci Rev.* **93**, 581.
Sáiz, A., Ruffolo, D., Rujiwarodom, M., Bieber, J. W., Clem, J., Evenson, P., Pyle, R., Duldig, M. L., Humble, J. E.: 2005, *29th Int. Cosmic Ray Conf.* **1**, 229.
Scherrer, P. H., Bogart, R. S., Bush, R. I., Hoeksema, J. T., Kosovichev, A. G., Schou, J., *et al.*: 1995, *Solar Phys.* **162**, 129.
Share, G. H., Murphy, R. J., Smith, D. M., Shih, A. Y., Hurford, G. J., Schwartz, R. A., Tylka, A. J., Lin, R. P.: 2006, AAS SPD Meeting, Abstract #28.06.
Silva, A. V. R., Wang, H., Gary, D. E.: 2000, *Astrophys. J.* **545**, 1116.
Simnett, G. M.: 2006, *Astron. Astrophys.* **445**, 715.
Slemzin, V., Kuzin, S., Bogachev, S.: 2005, In: Danesy, D., Poedts, S., De Groof, A., Andries, J. (eds.), *The Dynamic Sun: Challenges for Theory and Observations, Proc. 11th European Solar Phys. Meeting, ESA SP-600*, 166.
Somov, B. V.: 1992, *Physical Processes in Solar Flares*, Kluwer Academic Publ., Dordrecht.

Somov, B. V.: 2006, *Solar System Res.* **40**, 85.
Somov, B. V., Bogachev, S. A.: 2003, *Astron. Let.* **29**, 621.
Su, Y. N., Golub, L., Van Ballegooijen, A. A., Gross, M.: 2006, *Solar Phys.* **236**, 325.
Švestka, Z.: 2001, *Space Sci Rev.* **95**, 135.
Torii, C., Tsukiji, Y., Kobayashi, S., Yoshimi, N., Tanaka, H., Enome, S.: 1979, *Proc. Res. Inst. Atmospherics* **26**, Nagoya Univ., 129.
Tylka, A. J., Cohen, C. M. S., Dietrich, W. F., Lee, M. A., Maclennan, C. G., Mewaldt, R. A., Ng, C. K., Reames, D. V.: 2005, *Astrophys. J.* **625**, 474.
Uralov, A. M., Grechnev, V. V., Hudson, H. S.: 2005, *J. Geophys. Res.* **110**, A05104.
Vršnak, B., Gopalswamy, N.: 2002, *J. Geophys. Res.* **107**(A2), SSH 2-1.
Webb, D. F., Lepping, R. P., Burlaga, L. F., DeForest, C. E., Larson, D. E., Martin, S. F., Plunkett, S. P., Rust, D. M.: 2000, *J. Geophys. Res.* **105**, 27251.
White, S. M., Thomas, R. J., Schwartz, R. A.: 2005, *Solar Phys.* **227**, 231.
Zarro, D. M., Sterling, A. S., Thompson, B. J., Hudson, H. S., Nitta, N.: 1999, *Astrophys. J.* **520**, L139.
Zhang, J., Dere, K. P.: 2006, *Astrophys. J.* **649**, 1100.